Physics – Uspekhi **57** (12) 1180 – 1198 (2014)

REVIEWS OF TOPICAL PROBLEMS PACS numbers: **75.25. – j**, 75.30.Gw, 76.30.Fc

Anisotropic interactions in magnetic crystals with S-state ions. Nanostructures

S G Ovchinnikov, V V Rudenko

DOI: 10.3367/UFNe.0184.201412b.1299

Contents

1. Introduction **1180**

2. Description of the magnetic anisotropy of crystals **1181**

2.1. Phenomenological description of the magnetic anisotropy of rhombohedral, hexagonal, and tetragonal antiferromagnetic crystals; 2.2 Phenomenological description of the magnetic anisotropy of cubic ferro- and ferrimagnetic crystals; 2.3 'Microscopic' sources of magnetic anisotropy. Theoretical description; 2.4 Experimental investigation of anisotropic interactions in rhombohedral diamagnetic crystals with impurity S-state ions; 2.5 Anisotropic interactions in paramagnetic and magnetically ordered dielectrics with S ions; 2.6 Sources of uniaxial and hexagonal anisotropy in magnetically concentrated crystals with S-state ions. Generalized independent method of proper quantitative description of magnetic anisotropy

3. Multiferroic bismuth ferrite. Possibilities of the uniaxial anisotropy investigation (with the use of a diamagnetic analog with an Fe^{3+} impurity) in the parameter region of the spin cycloid existence in $BiFeO_3$ **1192**

4. Anisotropic interactions and nanostructures. Skyrmions **1193**

5. Conclusions **1197**

References **1197**

Abstract. Anisotropy mechanisms in compounds with S-state ions are discussed, including the 'single-ion' exchange mechanism that was developed theoretically by Nikiforov and coworkers based on the two-ion model and which has only recently received detailed experimental study. Results demonstrating the significant role of the 'single-ion' source are presented. An independent generalized method for quantitatively describing and predicting the anisotropy of magnetically ordered crystals is discussed, and its potential for the investigation of the $BiFeO_3$ multiferroic in the region of the existence of a spin cycloid is examined. The anisotropic interactions responsible for the formation of nanostructures in the form of spin vortices (skyrmions) in MnSi and Cu_2OSeO_3 are analyzed.

1. Introduction

The possibility to practically apply magnetic materials depends substantially on the magnitude and character of anisotropic interactions, which can be reasonably predicted based on experimental and theoretical investigations.

In this review, we mainly consider magnetically ordered compounds for which the parameters of spin Hamiltonians required for quantitatively assessing anisotropy have been established. These parameters are usually extracted from electron paramagnetic resonance (EPR) spectra on diamagnetic analogs with impurity ions of a magnetically concentrated substance. Based on such data obtained for magnetically ordered compounds, we generalize the results of the anisotropy investigations available in the literature.

The use of isostructural diamagnetic analogs is the only experimental method for verifying models that are used to calculate anisotropy fields. The cations of diamagnetic analogs have a completely filled outer electron shell (which is, consequently, more inert with respect to impurities) and the same charge as that in a magnetically ordered crystal. These compounds are characterized by a high degree of ionicity, which follows from monotonic dependences of the constants of spin Hamiltonians on lattice parameters. Therefore, in the case of the coincidence of lattice parameters [or of their ratios (see Fig. 2 in Section 2.4.1)] of a diamagnetic analog and a magnetically ordered substance, the magnitude and the symmetry of the crystal electric fields can be reproduced with good accuracy. However, it is frequently difficult to find a diamagnetic analog with lattice parameters close to those of a magnetically ordered crystal. Therefore, if possible, a series of diamagnetic crystals with an impurity is used, for which the dependence of constants of the spin Hamiltonian on some parameter (e.g., on the lattice parameter) is constructed. Such an approach has sufficiently long been used for estimating the contribution from the single-ion mechanism.

In this review, in particular, we give the results of the investigation of the behavior of single (isolated) ions and pairs of ions. The theory of the single-ion model for cubic crystals

S G Ovchinnikov, V V Rudenko Kirenskii Institute of Physics, Siberian Branch of the Russian Academy of Sciences, Akademgorodok 50, str. 38, 660036 Krasnoyarsk, Russian Federation
E-mail: sgo@iph.krasn.ru, rvv@iph.krasn.ru

Received 21 December 2013, revised 21 June 2014
Uspekhi Fizicheskikh Nauk **184** (12) 1299 – 1318 (2014)
DOI: 10.3367/UFNr.0184.201412b.1299
Translated by S N Gorin; edited by A M Semikhatov

was developed by Wolf [1]. The theory of 'single-ion' exchange anisotropy based on the two-ion model was developed by Nikiforov et al. [2]. Upon calculating the contribution from the two-ion mechanism to the anisotropy field of a magnetically ordered crystal using EPR data, a pair of interacting paramagnetic ions in diamagnetic compounds was first taken into account; then, in accordance with the definition of a magnetically concentrated substance, the sum over nearest neighbors was taken (see Sections 2.4.2 and 2.4.3).

The 'conventional' compounds chosen for the investigations differ in the crystal and magnetic structures. From the standpoint of crystal structure, these are cubic, hexagonal (trigonal), and tetragonal materials. For magnetic structures, these are paramagnetic crystals representing diamagnetic matrices with $3d^5$ or $4f^7$ ions introduced into them to ensure the possibility of observing the fine structure of the EPR spectra of isolated ions or pairs of ions. Magnetically ordered crystals are antiferromagnets (including one-dimensional), ferrites, and ferromagnets. Notably, MnF_2, EuO, $Y_3Fe_5O_{12}$, $(CH_3)_4NMnCl_3$, $MnCO_3$, $FeBO_3$, and α-Fe_2O_3 belong to these 'conventional' compounds. In this review, we also consider compounds (in particular, rhombohedral $YFe_3(BO_3)_4$) that have recently been studied experimentally by the research groups of Mukhin [3] and Pankrats [4]. These compounds have served as a basis for developing a generalized independent experimental method of quantitative description and prediction of magnetic anisotropy of crystals (see Section 2.6).

For a number of compounds that have been intensely studied in recent years (in particular, multiferroic $BiFeO_3$, dielectric Cu_2OSeO_3, and metallic MnSi), we discuss anisotropic interactions (Sections 3 and 4). In the last two compounds, a lattice of nanostructured spin vortex formations called skyrmions is observed. We note the importance of anisotropic interactions in $BiFeO_3$ and crystals with nanostructures, including in the formation of skyrmions.

As the theoretical tool in this review, we mainly use the method of spin Hamiltonians, which, according to recent data, can also be applied to MnSi (the description of the properties of this compound can be based on S-like wave functions of magnetic ions (see Section 4)) and to Cu_2OSeO_3. Based on spin Hamiltonians, we considered three sources responsible for the magnetic anisotropy of crystals with ions in the S state: dipole, single-ion, and 'single-ion' exchange (symmetric anisotropic exchange), as well as the antisymmetric anisotropic exchange interaction — the Dzyaloshinskii–Moriya interaction.

Ions in the S state have half-filled d and f electron shells, which are formally spherical and have zero orbital moment. However, an impurity of higher states leads to the appearance of an orbital moment, distortion of the electron cloud, and, as a consequence, the interaction of the ion spin of the compound with the crystal field via the spin–orbit coupling (which provides the nature of single-ion anisotropy). The nature of the 'single-ion' exchange mechanism consists in a change in the overlap of the orbital wave functions of a pair of ions upon rotating the spin. In [2], the change in the spin due to the impurity of upper states and, consequently, the change in the magnitude of the exchange interaction in the pair of ions were taken into account; in the usual single-ion mechanism, such a change is neglected. The 'single-ion' exchange anisotropy was obtained in the third order of the perturbation theory. In this case, the matrix elements depend linearly on the isotropic exchange interaction and quadratically on the spin–orbit coupling. The energy of this kind of anisotropy can be represented as a function of individual spins [2]. For a strong exchange interaction between the ions of the pair, the operators of the Hamiltonian can also be written in terms of the total spin $\mathbf{S} = \mathbf{s}_1 + \mathbf{s}_2$ (see Section 2.4.2).

Owing to [2] and the method of the investigation of the 'single-ion' exchange mechanism (with the use of diamagnetic analogs [see Sections 2.4.2–2.4.4)], it has become possible to add two new parameters to the constants of the spin Hamiltonian of the pair: the 'single-ion' exchange parameter and a constant that describes the contribution due to the distortion of the diamagnetic 'host' lattice by a 'foreign' impurity pair. This allowed solving the problem of the 'discrepancy' between the single-ion constants extracted from the single-ion and pair EPR spectra of diamagnetic crystals with an impurity of paramagnetic ions.

Antiferromagnetic resonance (AFMR) is typically used as the experimental method. The sign of the Dzyaloshinskii–Moriya interaction was recently determined (see Section 2.6) by the method of diffraction of synchrotron radiation interacting with the electric and magnetic systems of the crystal. For the observation of skyrmions in the corresponding compounds, methods such as small-angle neutron scattering (SANS), the Hall effect, and Lorentz microscopy are typically used.

In addition, we discuss the possibility of investigating magnetic anisotropy in the region of the existence of a spin cycloid [5] in rhombohedral multiferroic $BiFeO_3$, which is a promising material for use in various engineering devices [5–8]. The number of studies devoted to the investigation of this compound has grown intensely in recent years (see, e.g., [7, 8] and the references therein).

2. Description of the magnetic anisotropy of crystals

2.1. Phenomenological description of the magnetic anisotropy of rhombohedral, hexagonal, and tetragonal antiferromagnetic crystals

The magnetic properties of rhombohedral antiferromagnetic crystals with the structure of calcite ($FeBO_3$, $MnCO_3$) and corundum (α-Fe_2O_3) are described by the Dzyaloshinskii theory [9]. The magnetic structure of these crystals can be described in terms of two sublattices. According to [9], the free energy can be expanded in a series in powers of the vectors of reduced magnetization $\mathbf{m} = (\mathbf{M}_1 + \mathbf{M}_2)/M$ and antiferromagnetism $\mathbf{l} = (\mathbf{M}_1 - \mathbf{M}_2)/M$, where $M = 2|\mathbf{M}_1| = 2|\mathbf{M}_2|$. The expansion of the free energy up to fourth-order terms in a polar coordinate system related to the crystal axes ($z||c_3, y||c_2$) is written as [9, 10]

$$\begin{aligned}\Phi = {} & \frac{1}{2}\,B\mathbf{m}^2 + \frac{1}{2}\,a\cos^2\theta + \frac{1}{2}\,c\cos^4\theta + \frac{1}{2}\,bm_z^2 \\ & + d\sin\theta(m_y\cos\varphi - m_x\sin\varphi) \\ & + q\sin^3\theta\cos\theta\cos(3\varphi) + tm_z\sin^3\theta\sin(3\varphi) \\ & + e\sin^6\theta\cos(6\varphi)\,, \end{aligned} \tag{1}$$

where B is the exchange constant, a and c are the respective constants of uniaxial anisotropy of the second and fourth order, b is the uniaxial anisotropy constant of the antiferromagnetism vector, d is the Dzyaloshinskii constant, q is the

constant of hexagonal anisotropy, t is the constant of the hexagonal anisotropy of the antiferromagnetism vector, and e is the constant of hexagonal anisotropy of the sixth order. The angle θ (for the antiferromagnetism vector) of the polar coordinate system is counted from the c_3 axis, and the angle φ is counted from the symmetry plane of the crystal (the x axis).

The first term in the right-hand side of (1) characterizes the exchange energy of the crystal; the second, third, and fourth terms describe the uniaxial anisotropy; the fifth term corresponds to the Dzyaloshinskii interaction, which leads to the appearance of weak (itinerant-electron) ferromagnetism; and the last three terms describe the anisotropy energy in the basal plane.

The second and third terms in the right-hand side of (1) can be used to describe the uniaxial anisotropy in antiferromagnetic hexagonal and tetragonal crystals, in particular, in $(CH_3)_4NMnCl_3$ and MnF_2, and in rhombohedral $YFe_3(BO_3)_4$.

2.2 Phenomenological description of the magnetic anisotropy of cubic ferro- and ferrimagnetic crystals

We choose the yttrium iron garnet $Y_3Fe_5O_{12}$ and the ferromagnetic EuO as representatives of cubic crystals considered in this review.

The magnetic anisotropy of cubic ferro- and ferrimagnetic crystals can be expressed in terms of the free energy Φ, which is a function of direction cosines of the magnetization vector relative to the crystallographic axes. The free energy Φ can be written as the series [11]

$$\Phi = K_0 + K_1(\alpha_1^2\alpha_2^2 + \alpha_2^2\alpha_3^2 + \alpha_3^2\alpha_1^2) + K_2\alpha_1^2\alpha_2^2\alpha_3^2\,, \qquad (2)$$

where K_1 and K_2 are the first and second anisotropy constants, and α_n are the direction cosines.

The anisotropy constants for garnet are written as $K_i = K_{ia} + K_{id}$, where the indices a and d refer to the respective octahedral and tetrahedral sublattices, and $i = 1, 2$ indicates the order of the constant. The resulting anisotropy field can be written as $H_{iA} = (M_a H_{ia} + M_d H_{id})/M$, where $M = M_a + M_d$ is the total magnetization, $H_{ij} = K_{ij}/M_j$, and j = a, d.

2.3 'Microscopic' sources of magnetic anisotropy. Theoretical description

An important source of anisotropy in low-symmetry crystals is given by long-range dipole interactions; a second source, which is characteristic of all compounds with S-state ions, is the single-ion interaction; and a third mechanism is the anisotropic exchange.

Quantitative estimates based on the single-ion model [1] for $Y_3Fe_5O_{12}$ [12], EuO [13], α-Fe_2O_3, $FeBO_3$, and $MnCO_3$ [14–16] (with the use of constants of the spin Hamiltonian extracted from a series of isostructural diamagnetic analogs with impurities of isolated ions Fe^{3+}, Eu^{2+}, and Mn^{2+}) with the dipole interaction taken into account have shown substantial discrepancy with experimental data obtained on magnetically concentrated crystals. In view of these discrepancies and a number of analogous results obtained for other compounds, doubts appeared about the correctness of parameters extracted from the data on the investigation of an isostructural diamagnetic crystal, presumably because of significant lattice distortions introduced by isolated ions of the magnetically concentrated substance. Analogously, the validity of the single-ion model and thereby the possibility of obtaining reliable quantitative estimates based on this model were doubted, because this model, although based on quantum mechanical calculations, contains some elements of molecular field theory [17, 18]. The possible cause of the discrepancy with the experimental data can be the neglect of the 'single-ion' exchange anisotropy in these compounds.

The quantitative discrepancies between the single-ion model and the results of experiments have led, on the one hand, to the appearance of new experimental studies; the first was performed on yttrium iron garnets magnetically diluted by gallium, in which case an effect of the exchange field on the constants of the spin Hamiltonian of the Fe^{3+} ion was revealed [19]. On the other hand, theoretical study appeared [2] in which the authors calculated the magnetic anisotropy using a two-ion model within the perturbation theory, using exchange and spin–orbit interactions as the perturbing terms. In this model, the anisotropy appears in the third order of the perturbation theory, where the matrix elements are linear in the energy of the exchange interaction and are quadratic in the energy of spin–orbit coupling. In [2], a spin Hamiltonian describing anisotropic interactions was obtained in the form of expressions that couple tensor operators, which can be formally represented as equivalent spin operators [20, 21]. In this case, the expansion in irreducible tensor operators gives expressions containing the single-ion exchange anisotropy, which can be represented as a function of an isolated spin and, according to the authors of [2], this function can be quite significant in crystals with S-like ions. However, paper [2] has long remained unnoticed by experimentalists.

The physical reason for the magnetic anisotropy caused by anisotropic exchange interactions is the changes (upon rotation of the spins $\mathbf{s}_i$ and $\mathbf{s}_j$) in the overlap of orbital wave functions and, consequently, in the strength of the electrostatic interaction of both ions; as a result, the energy becomes dependent on the orientations of $\mathbf{s}_i$ and $\mathbf{s}_j$ relative to the crystal axes. It has long been assumed that such a mechanism of symmetric anisotropic exchange cannot make a significant contribution to magnetic anisotropy in compounds with S-state ions.

Qualitatively new information on the nature of anisotropic interactions can be obtained through the experimental investigation of pairwise interactions of paramagnetic ions in diamagnetic crystals. However, so far there have been only four experimental studies [22–25] on pairs of Mn^{2+} ions with a sufficiently full identification of the fine structure of the EPR spectra. Studies of this type on Fe^{3+} ions appeared only recently.

2.3.1. Dipole contribution to the magnetic anisotropy of rhombohedral, hexagonal, and tetragonal crystals. Rhombohedral, hexagonal, and tetragonal crystals belong to the class of crystals with relatively low symmetry, in which the contribution from magnetic dipole interactions to anisotropy is quite important.

The problem of the calculation of the energy of dipole interactions in crystals is related not only to the conditional convergence of lattice sums, which, using existing methods [26], can be transformed into quite rapidly converging series, but also to the clumsiness of these expressions, which can lead to errors in calculations. Therefore, for obtaining reliable information on dipole fields in crystals of $FeBO_3$, FeF_3, and $MnCO_3$, the dependences of these sums on the lattice parameters of the crystals have been constructed [14, 27]. The values of the dipole fields of uniaxial anisotropy

for the antiferromagnetism vector $H_{\rm Adip}$ of the compounds under consideration are given in Table 2 (see Section 2.6).

The deviations of the calculated values from the experimental data can be related to the existence of contributions from other mechanisms to the effective fields of the uniaxial anisotropy of these crystals. The most probable additional deviations can be due to the coupling of spin to the electric fields of the crystal. It follows from [12, 13, 28, 29] that this source makes a significant contribution to the anisotropy of cubic crystals and of the majority of uniaxial crystals. The single-ion source, in particular, can be dominating for the basal anisotropy of rhombohedral crystals. This assumption is supported by the dependence of the positions of lines in the EPR spectra observed in crystals that are isostructural to calcite with impurities of Mn^{2+} [30] and Fe^{3+} [31] on the rotation of the constant magnetic field about the threefold symmetry axis at an angle to the (111) plane. The contribution of the single-ion mechanism to the hexagonal anisotropy of rhombohedral weakly ferromagnetic crystals was calculated in [32–34].

2.3.2 Single-ion energy of hexagonal magnetic anisotropy in rhombohedral weakly ferromagnetic crystals. The crystal structure of $(CH_3)_4NMnCl_3$ was determined in [35]; that of rhombohedral $FeBO_3$ crystals is given, e.g., in [14]; that of $MnCO_3$ and α-Fe_2O_3 can be found in [36].

Calculations performed in [14, 32, 33] based on a pure (impurity-free) $FeBO_3$ crystal must also be valid for a description of the uniaxial and hexagonal anisotropy of manganese carbonate and hematite. The expressions for the uniaxial anisotropy constants in $(CH_3)_4NMnCl_3$ and MnF_2 (its crystal structure is given in [37]) coincide with the analogous expressions for rhombohedral crystals.

Figure 1 shows two nonequivalent positions in the lattice of the $FeBO_3$ crystal. The nonequivalence of positions 1 and 2 is due to different orientations of the BO_3 groups in the plane perpendicular to the threefold axis of the crystal. The BO_3 groups are shown in Fig. 1 as circles (atoms) connected by straight lines; atom B at the center is surrounded by three symmetrically located O atoms. The BO_3 groups shown in black lie above the plane of the figure; the open groups lie below the figure plane. One of the symmetry planes of the crystal passing through the octahedral complexes 1 and 2 formed by the ligands is shown with a thin solid line.

The distribution of the axes of the axial and cubic fields for the two nonequivalent positions of Fe^{3+} ions can be found from considering the symmetry of octahedral complexes. The mutually perpendicular cubic axes ξ_j, η_j, and ζ_j of the crystal field are denoted by arrows. The solid arrows correspond to a positive projection onto the z axis; the dashed arrows correspond to negative projection (the z axis is perpendicular to the figure plane). The projections of the axes ξ_1, η_1, and ζ_1 and of the axes ξ_2, η_2, and ζ_2 onto the (111) plane are misoriented and deviate from the symmetry planes of the crystal in the xyz system (with the origin placed at ion 1) by the respective angles $\alpha_{\rm cf1} = \alpha$ and $\alpha_{\rm cf2} = -\alpha$. The angles $\alpha_{{\rm cf}j}$ are counted from the projections of the cubic field axes onto the plane (111) toward the x axis; rotation from the x axis toward the y axis is assumed to be positive; the subscripts $j = 1, 2$ correspond to positions 1, 2. The axial components of the crystal field of the complexes coincide with one another and are oriented along the threefold axis of the crystal. Such an arrangement of the axes in crystals with a calcite structure is confirmed by the EPR data [14, 30, 31].

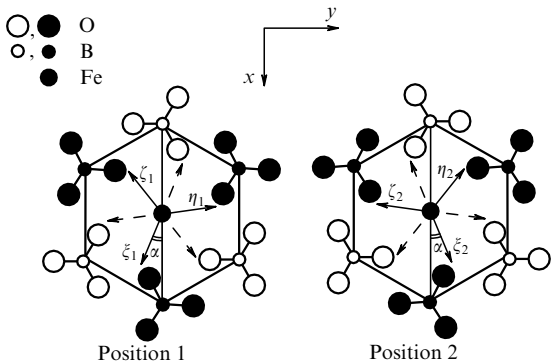

Figure 1. Arrangement of cubic axes of the crystal field for two nonequivalent positions of the ion M in the lattice of MBO_3 (M = Fe, Ga, In, Lu, Sc) [14, 31].

According to [14, 30, 32, 33], the spin Hamiltonian in a coordinate system xyz with the origin placed at the jth ion can be written as

$$\mathcal{H} = \sum_{j=1}^{2} \left\{ g\mu_{\rm B} \mathbf{H}_j^{\rm eff} \mathbf{s}_j + \frac{1}{3} D_{\rm cf} O_{2j}^0 + \frac{F_{\rm cf}}{180} O_{4j}^0 - \frac{a_{\rm cf}}{180} \left[O_{4j}^0 - 20\sqrt{2} \left(\cos(3\alpha_{{\rm cf}j}) O_{4j}^3 - \sin(3\alpha_{{\rm cf}j}) \tilde{O}_{4j}^3 \right) \right] \right\}, \quad (3)$$

where $D_{\rm cf}$ and $F_{\rm cf}$ are the respective axial constants of the second and fourth order, $a_{\rm cf}$ is the constant of the cubic crystal field, g is the spectroscopic splitting factor, which is assumed to be isotropic, $\mu_{\rm B}$ is the Bohr magneton, $\mathbf{H}_j^{\rm eff}$ is the exchange field at the jth ion or the external magnetic field $\mathbf{H}$ (depending on which crystal is considered: magnetically concentrated or diamagnetic with an impurity of a paramagnetic ion), $\mathbf{s}$ is the spin of the ion, and O_n^m are equivalent spin operators, which have the form given, e.g., in [20]. The second and third terms in the right-hand side describe axial-symmetry interactions, and the subsequent terms describe cubic-symmetry interactions.

The temperature dependence of the hexagonal single-ion anisotropy calculated in [14, 32] is written as

$$H_{q\,{\rm cf}}({\rm Fe}^{3+}) \sin^6\theta \cos(6\varphi) = -\frac{a_{\rm cf}^2 \cos^2(3\alpha_{\rm cf})\, r^2(Y)}{18\left(H_{\rm A}(0) + H_{\rm D}^2(0)/H_{\rm E}(0)\right) B_s^3(x)\, s^2} \sin^6\theta \cos(6\varphi), \quad (4)$$

where the constant $a_{\rm cf}$ is expressed in oersteds, the angle $\alpha_{\rm cf}$ is expressed in degrees, $r(Y)$ is the function of temperature introduced by Wolf [1] (also see, e.g., [14, 32, 33]); $H_{\rm A}(0) = a(0)/M(0)$, $H_{\rm D}(0) = d(0)/M(0)$, $H_{\rm E}(0) = B(0)/M(0)$, s is the spin quantum number, equal to 5/2, and $B_s(x)$ is the Brillouin function. For $H_{\rm A}(T)$, the contribution of only the dipole interaction was taken into account because the single-ion and the 'single-ion' exchange contributions approximately compensate each other (see Table 2 in Section 2.6).

2.3.3. Impurity single-ion anisotropy in $FeBO_3$ crystals. Phenomenological consideration. The existence of a point of hexagonal anisotropy compensation in $FeBO_3$, its different magnitudes for different samples at low temperatures, and a

significant increase in the width of the AFMR line at $T \leqslant 20$ K indicate the presence of impurities [14, 32–34]. In addition, the presence of an impurity manifests itself in the occurrence of uniaxial anisotropy in the basal plane of $FeBO_3$ crystals, which is observed by the AFMR method [14]. A significant uniaxial anisotropy in the basal plane appeared at temperatures below 30 K. Fe^{2+} ions can serve as impurities arising as a result of the appearance of vacancies at the sites of some BO_3^{3-} groups [38]. The boron ions are bound covalently with the oxygen ions; such a group can exist as an integral species in the molten solution at the temperatures of growth of the $FeBO_3$ crystal [38]. Because of a large spatial extension of the BO_3^{3-} groups, their incorporation into the crystal presents difficulties, which leads to the appearance of vacancies at the sites of these groups. The decrease in the negative charge in the crystal leads to the appearance of Fe^{2+} ions.

In [33, 34], a model of the behavior of a system consisting of an Fe^{2+} ion and a vacancy at the BO_3^{3-} site was suggested. In this model, after the vector of the external field rotates in the basal plane, an electron hops from the Fe^{2+} ion to the Fe^{3+} ion around the vacancy (coordination number 6). To explain the behavior of this system, the anisotropy tensor with triclinic symmetry was introduced and kinetic equations for the ferrite ions have been solved (the local point symmetry of the positions of the iron ions is c_1).

The solution of the kinetic equations has shown that after the rotation of the antiferromagnetism vector in the basal plane, the relaxation of the impurity subsystem starts at the instant $t = t_0$. At $t = \infty$, the system comes to equilibrium, and the contribution from Fe^{2+} to the hexagonal anisotropy is equal to $-D' \sin^3\theta' \cos\theta' \cos(3\varphi' - \psi)$ [33, 34]. Here, D' and ψ are respectively a constant and the phase angle, which depend on the parameters of the anisotropy tensor for the Fe^{2+} ions; θ' and φ' are the polar and azimuthal angles of the antiferromagnetism vector $\mathbf{l}' = (\mathbf{M}_1' - \mathbf{M}_2')/M'$ of the Fe^{2+} ions; $\mathbf{M}_1'$ and $\mathbf{M}_2'$ are the sublattice magnetizations; and $M' = 2|\mathbf{M}_1'| = 2|\mathbf{M}_2'|$. The free energy for Fe^{2+} in the $FeBO_3$ crystal (the impurity magnetic subsystem is in thermodynamic equilibrium with the Fe^{3+} subsystem) can be written as [33]

$$\begin{aligned}\Phi' = {} & A'(\sin\theta \sin\theta' \cos\varphi \cos\varphi' \\ & + \sin\theta \sin\theta' \sin\varphi \sin\varphi' + \cos\theta \cos\theta') \\ & + \frac{1}{2}\, a' \cos^2\theta' - D' \sin^3\theta' \cos\theta' \cos(3\varphi' - \psi)\,, \end{aligned} \qquad (5)$$

where A' is the constant of the isotropic exchange interaction between the Fe^{2+} and Fe^{3+} ions. The last two terms in the right-hand side of Eqn (5) describe the respective uniaxial and hexagonal anisotropies. The minimization of $\Phi + \Phi'$ gives the following expression for the total effective energy of the hexagonal anisotropy [33]:

$$\begin{aligned} & \omega_q \sin^6\theta \cos(6\varphi) = \omega_q(Fe^{3+}) \sin^6\theta \cos(6\varphi) \\ & + \omega_q(Fe^{2+}) \sin^6\theta' \cos(6\varphi' - 2\psi) \\ & = \omega_q(Fe^{3+}) \sin^6\theta \cos(6\varphi) - \frac{D'^2}{4a'} \sin^6\theta \cos(6\varphi - 2\psi)\,. \end{aligned}$$

We note that the constant D' is inversely proportional to the temperature.

Because the hexagonal anisotropy changes sign at the point of compensation, it follows that $\psi = 90^\circ$ (over the entire temperature range). For the uniaxial anisotropy constants, we have

$$\omega_A = (a + a') \cos^2\theta\,.$$

2.3.4 Impurity anisotropy. 'Microscopic' consideration. According to [17], the Fe^{2+} ion can exist in a singlet or doublet orbital ground state, depending on whether the potential of the axial electric field along the trigonal axis is minimum or maximum. This potential is given in [39]. The calculations performed in [40] have shown that the potential of the axial electric field along the trigonal axis should be minimum; then, according to [17, 41], the lower energy levels can be described by the effective spin $s = 1$.

The Hamiltonian for the impurity Fe^{2+} ion in the single-ion approximation in the case of the lowest symmetry is written as [20]

$$\begin{aligned}\mathcal{H} = {} & \sum_{j=1}^{2} \left(g\mu_B \mathbf{H}_j^{\text{eff}} \mathbf{s}_j + A_2^0 O_{2j}^0 + A_2^1 O_{2j}^1 \right. \\ & \left. + A_2^2 O_{2j}^2 + \tilde{A}_2^1 \tilde{O}_{2j}^1 + \tilde{A}_{2j}^2 \tilde{O}_{2j}^2\right). \end{aligned}$$

Expressions for the operators O_n^m are given, for example, in [20]. The solution of the eigenvalue problem for this Hamiltonian gives an expression for the energy levels obtained in the first-order perturbation theory [33]. The uniaxial anisotropy constant for the Fe^{2+} ion found from the expansion of the free energy can be expressed as

$$a'(Fe^{2+}) \cos^2\theta = 3Nc_0 A_2^0 \frac{z_1'}{z_0'} \cos^2\theta\,,$$

where N is Avogadro's number, c_0 is the concentration of the Fe^{2+} impurity, and the expressions for the functions z_0' and z_1' are given in [33].

The energy of the hexagonal effective anisotropy is written as

$$\omega_q'(Fe^{2+}) \sin^6\theta \cos(6\varphi) = \frac{Nc_0 B_{\text{imp}}}{(k_B T)^2} \frac{z_1'}{z_0'} \sin^6\theta \cos(6\varphi)\,,$$

where B_{imp} is a constant that includes the constants of the energy levels [33], and k_B is the Boltzmann constant.

2.3.5. Anisotropic exchange in hematite crystals. The interpretation of the temperature dependence of the effective anisotropy fields in hematite, unlike that in $FeBO_3$ and $MnCO_3$, is different in view of the difference in the crystal structures and, consequently, in the exchange fields. In the unit cell of hematite, two pairs of the most closely spaced iron ions whose axis coincides with c_3 provide the effective exchange field of this crystal with a good accuracy. This follows from the EPR measurements on pairs of Fe^{3+} and Cr^{3+} ions in the isostructural crystal of corundum [42, 43].

According to [2, 44], the Hamiltonian that describes uniaxial anisotropy for a pair of iron ions in hematite can be represented as

$$\begin{aligned}\mathcal{H} = {} & \sum_{j=1}^{2} g\mu_B \mathbf{H}_j^{\text{eff}} \mathbf{s}_j + A_{\text{ex}} O_{11}^0 O_{12}^0 \\ & + B_{\text{ex}} O_{21}^0 O_{22}^0 + C_{\text{ex}} O_{31}^0 O_{12}^0\,, \end{aligned} \qquad (6)$$

where the first term in the right-hand side represents the isotropic exchange energy in the molecular-field approximation; the other terms describe the energy of anisotropic exchange expressed in terms of irreducible tensor spin operators [20], which coincide in their form with equivalent spin operators, and A_{ex}, B_{ex}, and C_{ex} are the corresponding exchange constants. To simplify expression (6), we omit the parts corresponding to the 'single-ion' exchange anisotropy and single-ion anisotropy. The solution of the simplified problem is given in Sections 2.4.2 and 2.4.3. The uniaxial anisotropy fields of the first and second constants at an arbitrary temperature are as follows [45]:

$$H_A \cos^2\theta = \left[(A'_{dip} + A'_{ex})\,\frac{z_4}{5z_0} + B'_{ex}\,\frac{z_1^2}{5z_0z_4} + C'_{ex}\,\frac{z_3}{5z_0} + D'_c\left(-\frac{z_1}{z_4}\right) + E'_c\left(-\frac{5z_2}{z_4}\right)\right]\cos^2\theta\,,$$

$$H_c \cos^4\theta = -\left[\frac{3}{2}\,B'_{ex}\,\frac{z_1^2}{5z_0z_4} + \frac{25}{13}\,C'_{ex}\,\frac{z_3}{5z_0} + \frac{7}{6}\,E'_c\left(-\frac{5z_2}{z_4}\right)\right]\cos^4\theta\,. \qquad (7)$$

Here, $A'_{dip} = 10.04$ kOe [28] is the dipole field of the magnetically concentrated crystal at $T = 0$ calculated directly; A'_{ex}, B'_{ex}, and C'_{ex} are the fields of the anisotropic exchange corresponding to the constants A_{ex}, B_{ex}, and C_{ex} of Hamiltonian (6); D'_c is the single-ion plus 'single-ion' exchange anisotropy field (in total, the 'single-ion' field), which is determined by second-order invariants of Hamiltonian (3) as well as of Hamiltonian (8) given in Section 2.4.2; and E'_c is the 'single-ion' field corresponding to the fourth-order invariants of Hamiltonians (3) and (8). The expressions for $z_0 - z_4$ are given in [45]. Equation (7) also includes the expressions (which were omitted above) for the single-ion and 'single-ion' exchange [2, 14, 33] anisotropy (we note that they have identical operator structures).

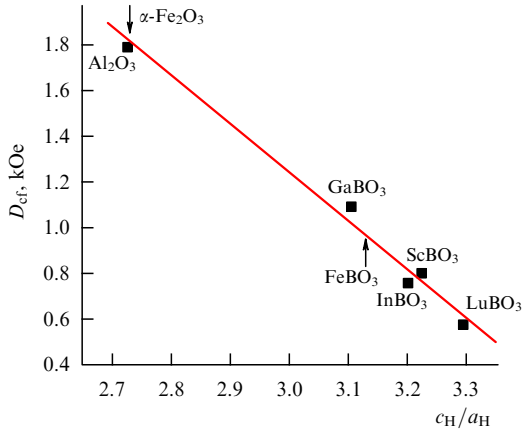

Figure 2. Variation of the constant D_{cf} of the spin Hamiltonian of the Fe^{3+} ion as a function of the ratio of the lattice parameters c_H/a_H of the hexagonal lattice in MBO_3 and Al_2O_3 crystals.

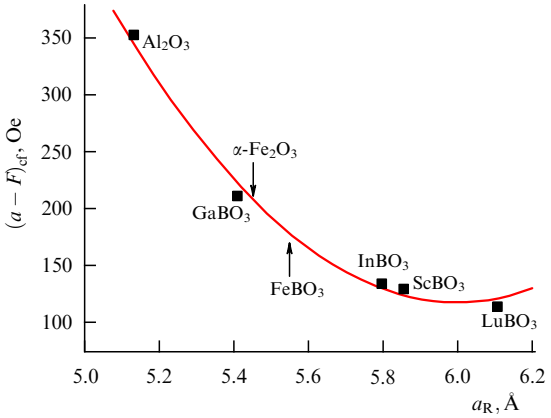

Figure 3. Dependence of the constant $(a - F)_{cf}$ of the spin Hamiltonian on the lattice parameter a_R of the rhombohedral lattice in $MBO_3 + Fe^{3+}$ and $Al_2O_3 + Fe^{3+}$ crystals.

2.4 Experimental investigation of anisotropic interactions in rhombohedral diamagnetic crystals with impurity S-state ions

2.4.1 Electron paramagnetic resonance of isolated ions in isostructural crystals $MBO_3 + Fe^{3+}$ (M = Ga, In, Lu, Sc). The most detailed investigations of anisotropic interactions in diamagnetic crystals with impurity S-state ions are the investigations of isolated ions using the EPR method. However, dedicated investigations of the anisotropy of magnetically concentrated substances based on EPR studies of isolated ions are scarce. The EPR investigations of isolated Fe^{3+} ions in a series of isostructural diamagnetic garnets [12, 46] are the only dedicated work of this kind.

The electron paramagnetic resonance of isolated ions has been well studied in some isostructural $MBO_3 + Fe^{3+}$ crystals (M = Ga, In, Lu, Sc), and we here give only the main results [14, 31]. Figures 2 and 3 display the dependences of the constants of spin Hamiltonian (3) on the lattice parameters obtained by the EPR method in $MBO_3 + Fe^{3+}$ crystals (M = Ga, In, Lu, Sc).

In the literature, identifications of pair spectra of Fe^{3+} ions have long been absent. In view of the insufficient study of pairwise interactions by the EPR method, the constants extracted from experimental data have not been interpreted either. For the same reason, the relation between the constants of spin Hamiltonians of isolated ions and pairs has not been established. No experimental or methodological applications of the data obtained on pairs for magnetically concentrated crystals have been obtained.

2.4.2 Electron paramagnetic resonance of pairs of Fe^{3+} ions in MBO_3 crystals (M = Ga, In, Lu, Sc). The elements of the crystal and magnetic structures of the $MBO_3 + Fe^{3+}$ crystals that play an important role in interpreting the EPR pair spectra are as follows. The first pair of nearest exchange-coupled Fe^{3+} ions is antiferromagnetic. Two other Fe^{3+} ions more distant from the central Fe^{3+} ion (next-to-nearest neighbors) form two ferromagnetically coupled pairs with the central ion.

The strong isotropic exchange in an antiferromagnetically coupled pair results in the formation of six multiplets in the case of the total spin $S = 5$. The energies of these states can be written as [22]

$$E_S = \frac{J}{2}\left[S(S+1) - s_i(s_i+1) - s_j(s_j+1)\right],$$

where J is the constant of the exchange interaction of the pair, and S, for each multiplet of the pair, takes one of the values $s_i + s_j$, $s_i + s_j - 1, \ldots$, $s_i - s_j$, where s_i and s_j are the spin quantum numbers of the ions of the pair equal to 5/2.

The Hamiltonian for each multiplet of the antiferromagnetically coupled pair in a diamagnetic crystal with the energy E_S, where the vector of the external field is oriented along the threefold axis c_3, can be represented, according to [22, 33, 47–50], as follows:

$$\mathcal{H} = g\mu_B H S_z + \frac{D_S}{3} O_2^0(S_z) - \frac{(a-F)_{cS}}{180} \gamma_S O_4^0(S_z), \qquad (8)$$

where H is the external magnetic field ($\mathbf{H}||z$), S_z is the projection of the total spin operator $\mathbf{S}$ (of the pairs of Fe^{3+} or Mn^{2+} ions) onto the z axis, $D_S = 3\alpha_S D_{dip} + \beta_S D_{cS}$, $\alpha_S = (1/2)[S(S+1) + 4s_i(s_i+1)]/(2S-1)(2S+3)$, $\beta_S = [3S(S+1) - 3 - 4s_i(s_i+1)]/(2S-1)(2S+3)$, γ_S are nonlinear functions of S, which are given in [49, 50], $D_{dip} = (g^2\mu_B^2/2r_{ij}^3)(1 - 3\cos^2\theta_{ij})$ is the dipole interaction constant for the pair of ions in the point approximation, D_{cS} and $(a-F)_{cS}$ are the second-order and fourth-order 'single-ion' constants at the corresponding irreducible tensor operators O_2^0 and O_4^0, which include the contributions from the single-ion and 'single-ion' exchange mechanisms of anisotropy [2, 44], and θ_{ij} is the angle between the axis of the pair and the c_3 axis. The expressions for the operators O_n^m are given, for instance, in [20].

Each multiplet with the total spin S is located in the exchange field arising in the pairwise interaction. The expression for the exchange field at the multiplets of the pair is [33]

$$H^{ex} = \frac{1}{g\mu_B}\frac{\partial E_S}{\partial|\mathbf{S}|} = \frac{J}{g\mu_B}\sqrt{S(S+1)}\,.$$

The constant D_S can be represented as [33, 47]

$$D_S = 3\alpha_S D_{dip} + \beta_S\left[D_{c0} + D_{cf} + A\sqrt{S(S+1)}\right], \qquad (9)$$

where the first term in the square brackets is due to the distortions of the lattice of the diamagnetic crystal by the 'foreign' pair, the second term reflects the effect of the crystal field, the third term describes the dependence on the exchange field of the pair, and the constant A has the meaning of the 'single-ion' exchange parameter.

The experimental results for the constant D_S of the spin Hamiltonian in $MBO_3 + Fe^{3+}$ crystals can be represented as a function of S (Fig. 4) [48]. The results of the identification of the EPR spectra are given in Section 2.4.4.

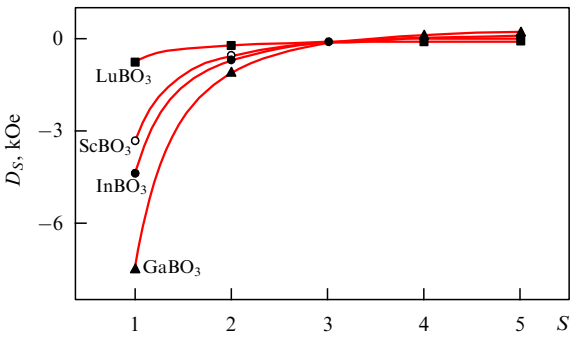

Figure 4. Dependence of the second-order axial constant D_S of the spin Hamiltonian of Fe^{3+} pairs in MBO_3 crystals on the total spin number S [48]. The different symbols denote experimental data; the solid curves correspond to the results of calculations.

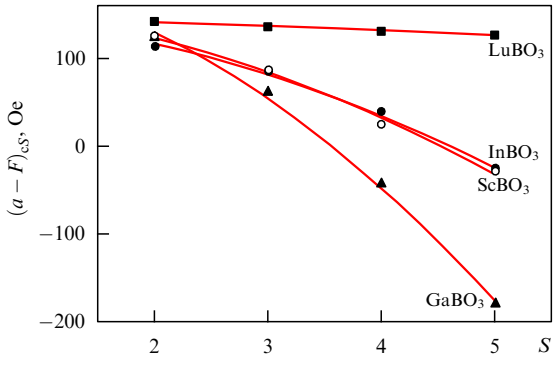

Figure 5. Dependence of the fourth-order axial constant $(a-F)_{cS}$ of the spin Hamiltonian of Fe^{3+} pairs in MBO_3 crystals on the total spin number S [48].

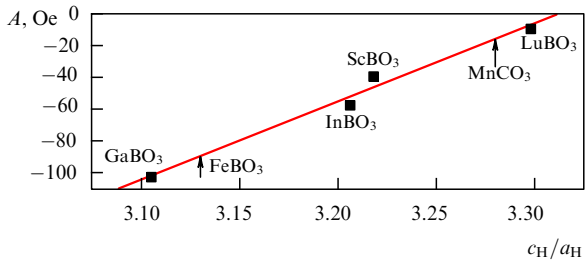

Figure 6. Dependence of the fitting 'single-ion' exchange parameter A for paired Fe^{3+} ions in MBO_3 crystals on the ratio of the lattice parameters of the hexagonal lattice c_H/a_H [48]. The arrows indicate the values of A corresponding to the $FeBO_3$ and $MnCO_3$ crystals.

Figure 5 displays the dependences of the fourth-order constant on the total spin number [48]. The curves correspond to the results of calculations using the expression

$$(a-F)_{cS} = (a-F)_{c0} + (a-F)_{cf} + BS(S+1), \qquad (10)$$

where B is the 'single-ion' exchange constant entering the fourth-order invariant in spin operators. The fourth-order 'single-ion' exchange invariant in spin operators does not follow from the abovementioned calculations [2, 44]; it can apparently be obtained in the perturbation theory approximations of a higher order compared to that assumed in [2, 44].

An analysis of the results indicates that in the zero exchange field, the magnitude of distortions introduced by pairs of Fe^{3+} ions is mainly determined by the deviations of the lattice parameters of the diamagnetic analog from the lattice parameters of $FeBO_3$ [48].

Figure 6 shows the linear dependence of the parameter A on the ratio of the lattice parameters of the hexagonal unit cell of MBO_3 crystals. The quadratic dependence of the parameter B on the lattice parameters is shown in Fig. 7.

2.4.3 Theoretical substantiation of the method for investigating the anisotropy of magnetically concentrated uniaxial crystals with the use of EPR data on pairs of ions. The results given in Section 2.4.2 and in this section for isolated pairs can be used to include the contributions from the constants of the pairwise interaction Hamiltonian to the magnetic anisotropy of $FeBO_3$, $MnCO_3$, and α-Fe_2O_3 antiferromagnetic crystals [33, 48]. To explain the relation between the parameters of the exchange energy of a pair of ions in a 'magnetically

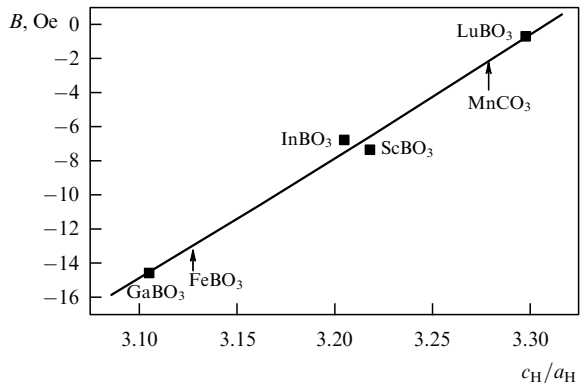

Figure 7. Dependence of the fitting 'single-ion' exchange parameter B for pairs of Fe^{3+} ions in MBO_3 crystals on the ratio of the lattice parameters of the hexagonal lattice c_H/a_H [33]. The arrows indicate the values of B corresponding to the $FeBO_3$ and $MnCO_3$ crystals.

concentrated' crystal, written in the approximation of molecular field theory, and of a pair of ions of a paramagnetic impurity in a diamagnetic substance, the following calculations were performed [33].

The exchange energy of the interaction of the ith ion in a magnetically concentrated crystal at $T = 0$ is expressed as $E(T = 0) = -nJs_is_j$, where n is the number of magnetically active nearest neighbors of the ith ion. Assuming that $n = n_0 = 1$ and equating the energies of two spins in the lattice to the energy of an isolated pair E_S,

$$E(T = 0, n_0) = E_{S\text{mc}}\,, \tag{11}$$

we find the value of the effective spin number S_{n0} of the pair of ions of the paramagnetic impurity in a diamagnetic substance, which corresponds to the energy of the lower level $E(T = 0)$ of the ith ion of a 'magnetically concentrated' crystal interacting with the jth ion. In Eqn (11) and below, the subscript mc in the notation for quantities that characterize the pairwise interactions and interactions of the spin of isolated ions with the crystal field means the coincidence of the lattice parameters (or their ratio) of the hypothetical diamagnetic analog with the corresponding quantities of the magnetically concentrated crystal.

The solution of quadratic equation (11) for S with $s_i = s_j = 5/2$ gives a value of the effective spin number that has a physical meaning, $S_{n0} = 1.79$. Then, summing over the neighbors of the ith ion in the molecular field approximation in the left-hand side of Eqn (11), we find the exchange energy of interaction of the ith ion with the nearest surroundings for the magnetically concentrated crystal at $T = 0$:

$$E(T = 0) = nE_{S\text{mc}}(S_{n0})\,. \tag{12}$$

The right-hand side of Eqn (12) can be presented as the energy of n pairs of paramagnetic impurities in a diamagnetic crystal, which corresponds to the exchange field

$$H^{\text{ex}} = n\,\frac{J}{g\mu_{\text{B}}}\,\sqrt{S_{n0}(S_{n0}+1)}\,. \tag{13}$$

Taking Eqn (13) into account and determining the parameters A_{mc} and B_{mc} (see Figs 6 and 7), we calculate the 'single-ion' constants of the spin Hamiltonian for the magnetically concentrated crystal [33]:

$$D_{\text{mc}} = D_{\text{cfmc}} + nA_{\text{mc}}\sqrt{S_{n0}(S_{n0}+1)} = D_{\text{cfmc}} + 2.26nA_{\text{mc}}\,,$$

$$(a-F)_{\text{mc}} = (a-F)_{\text{cfmc}} + nB_{\text{mc}}S_{n0}(S_{n0}+1) = (a-F)_{\text{cfmc}} + 5.00nB_{\text{mc}}\,. \tag{14}$$

The 'single-ion' constants D_{mc} and $(a-F)_{\text{mc}}$, apart from the known contributions D_{cfmc} and $(a-F)_{\text{cfmc}}$ from isolated ions, also include the 'single-ion' exchange contributions. To write the effective anisotropy fields in rhombohedral antiferromagnetic crystals with 'single-ion' exchange contributions taken into account, their well-known single-ion expressions at $T = 0$ can be used. According to [33], the 'single-ion' contribution to the uniaxial-anisotropy fields (for the second-order and fourth-order constants) can be represented as

$$H_{A\text{mc}}(0) = 2\left(s-\frac{1}{2}\right)\left\{D_{\text{cfmc}} + 2.26nA_{\text{mc}} + \frac{1}{6}\,(s-1)\left(s-\frac{3}{2}\right)\left[(a-F)_{\text{cfmc}} + 5.00nB_{\text{mc}}\right]\right\},$$

$$H_{c\text{mc}}(0) = -\frac{7}{18}\left(s-\frac{1}{2}\right)(s-1)\left(s-\frac{3}{2}\right) \times \left[(a-F)_{\text{cfmc}} + 5.00nB_{\text{mc}}\right]. \tag{15}$$

Thus, when calculating the anisotropy parameters for a magnetic crystal in terms of the parameters of isolated and paired impurities in nonmagnetic crystals, an approximation for the Heisenberg exchange is used. However, for quasi-one-dimensional chains, for which the mean-field approximation is invalid, this approach is inapplicable. Indeed, in the limit of an isotropic Heisenberg chain, according to the Mermin–Wagner theorem, the magnetically ordered state is absent, whereas the mean-field approximation leads to an antiferromagnetic order, in particular, in $(CH_3)_4NMnCl_3$ (see Section 2.6, Table 2). Usually, the magnetic state in a one-dimensional chain can be stabilized by the existence of either anisotropy or weak interaction between the chains. In the case of the $(CH_3)_4NMnCl_3$ crystal, the stabilization of the antiferromagnetic order is assumed to be due to the anisotropy.

2.4.4 Method for identifying the EPR spectra of pairs of Fe^{3+} ions in MBO_3 crystals (M = Ga, In, Lu, Sc). The content of this section is based on [48]. In the literature, data on the experimental investigation of the fine structure of spectra of pairs of Fe^{3+} ions related to anisotropic interactions are absent.

In order to process the spectra, A N Sudakov (Institute of Computer Simulation, Siberian Branch, Russian Academy of Sciences) has developed a special computer program. For a given orientation of the crystal relative to **H**, the values of the total spin S are determined by the g factor ($g = 2$) and two axial constants of the Hamiltonian, D_S and $(a-F)_{cS}$. The equations corresponding to the values of the resonance fields for lines with the spin $S = 3, 4, 5$ are solved by the least-square method. Using the computer program, all possible variants of the sets of equations were enumerated and calculated. The results of the solutions of the variants considered were arranged in a certain sequence according to the magnitude of the root-mean-square error for the constants of the spin Hamiltonian. The program made it possible to identify the

lines described by corresponding equations of a given variant in the magnetic quantum number. With this method of processing the pair spectra, the choice of the best variant of the solution was determined by the following criteria: the smallest rms error; a good correspondence between the theoretical and experimental intensities of the lines (which, however, was not a decisive criterion, in view of the different values of the intensities in different samples of approximately the same weight (Fig. 8)); and the degree of monotonicity of the dependences of the spin Hamiltonian constants on S. In addition, to identify the spectra, an independent estimation of D_S was also used. For this, two extreme compositions (in terms of the lattice parameters) were selected among the compounds: $LuBO_3 + Fe^{3+}$ and $GaBO_3 + Fe^{3+}$. The first compound should exhibit weak exchange interaction in view of the symmetry of the lattice and magnitudes of its parameters, which follows from the data given in Fig. 6 (at $(c_H/a_H) \sim 3.3$, the exchange field is rather close to zero). Therefore, the parameter A in Eqn (9) can be taken equal to zero. The parameter D_{dip} can be calculated. The values of the single-ion constant D_{cf} are known (they are given, e.g., in [14, 31]). The constant D_{c0}, which characterizes the distortion of the diamagnetic matrix by a 'foreign pair', can be approximately estimated [48] as

$$\frac{\Delta D_{cf}}{\Delta(c_H/a_H)}\,0.169 = -2.6\times 10^3 \times 0.169 \text{ Oe} \,(\approx -440 \text{ Oe})\,,$$

where $\Delta D_{cf}/\Delta(c_H/a_H)$ is the increase in the single-ion constant of the spin Hamiltonian upon a corresponding increase in the lattice parameters $\Delta(c_H/a_H)$, which reflects the effective lattice distortions of the $MBO_3 + Fe^{3+}$ crystals [48]. The value 0.169 is the difference in the axial ratios c_H/a_H of $LuBO_3$ and $FeBO_3$. From the spectrum of resonance lines with $S = 5$ in $LuBO_3 + Fe^{3+}$, the value $D_{c0} = -660$ Oe was obtained.

The compound $GaBO_3 + Fe^{3+}$ has lattice parameters close to those of $FeBO_3$ and should therefore have approximately the same magnitudes of the pairwise and single-ion interactions. Hence, in Eqn (9), we can neglect the contribution from the distortions caused by a 'foreign' pair. In this case, the constant D_{cf} remains equal to 1078 Oe [14, 31, 48]. The 'single-ion' exchange contribution $2.26nA_{mc}$ and, consequently, the parameter A can be estimated from experimental data for the $FeBO_3$ crystal and be applied to $GaBO_3 + Fe^{3+}$ (the magnitude of this contribution is -86 Oe). Based on the EPR spectra, we obtained the value -100 Oe for the parameter A in $GaBO_3 + Fe^{3+}$. With the abovementioned factors and the obtained estimates taken into account, the constants of the spin Hamiltonian were found from the EPR spectrum at $S = 5-3$. From the dependences $D_{cS}(S) = D_{cf} + D_{c0} + A\sqrt{S(S+1)}$, and $(a-F)_{cS}(S) = (a-F)_{cf} + (a-F)_{c0} + BS(S+1)$, the values of D_{cS} and $(a-F)_{cS}$ at $S = 1,\ 2$ were then calculated with the use of fitting parameters, and the positions of the corresponding resonance lines in the spectrum were determined. If these lines were present (this was the fourth criterion), the final variant of the identification of the spectrum was assumed. The spectrum of pairs in $LuBO_3 + Fe^{3+}$ thus identified is shown in Fig. 8.

2.4.5. Investigation of the basal-plane anisotropy in $FeBO_3$ crystals by the method of antiferromagnetic resonance. The possibility of the existence of the hexagonal anisotropy predicted by the Dzyaloshinskii theory [9] in rhombohedral weakly ferromagnetic crystals has long been doubted (for compounds with S-state ions). The investigations performed

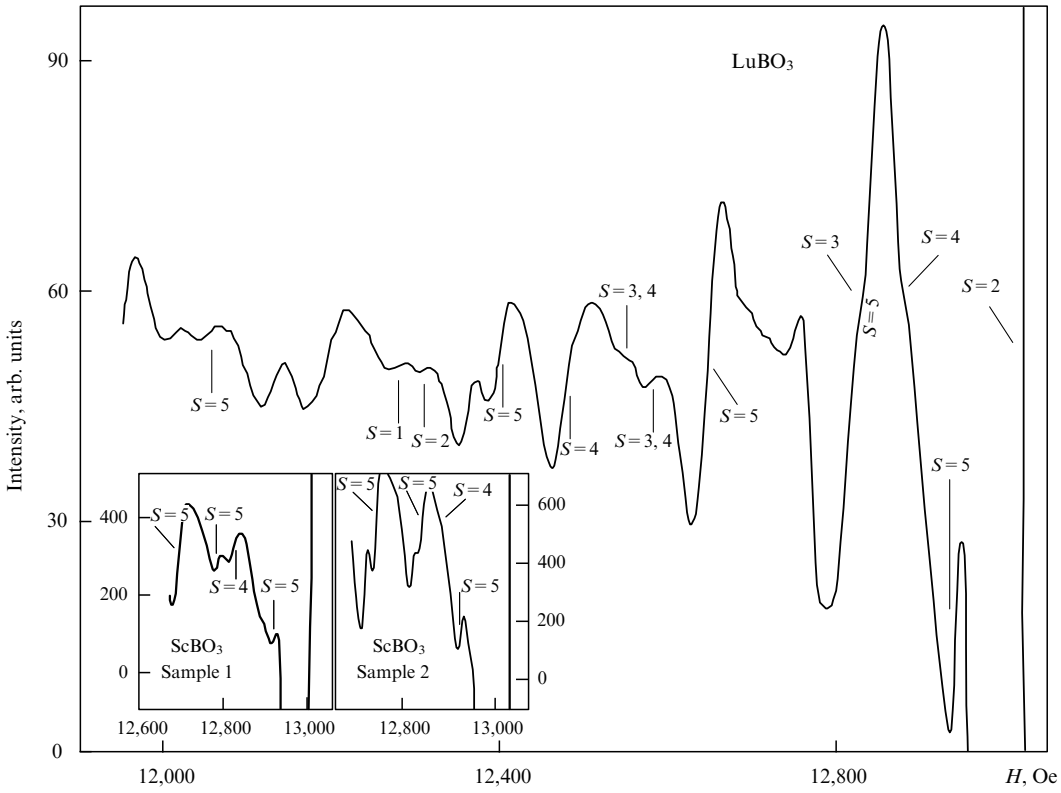

Figure 8. Identified EPR spectrum of antiferromagnetically coupled Fe^{3+} pairs in $LuBO_3$ crystals [48].

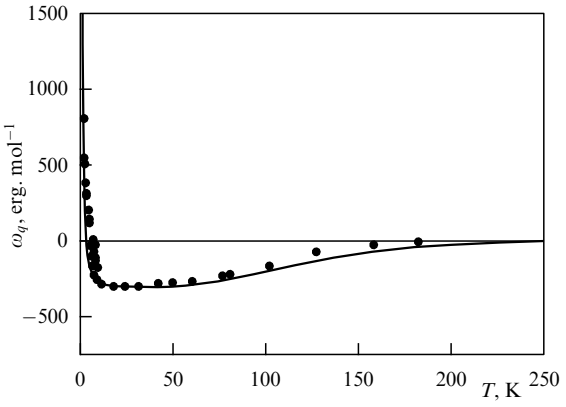

Figure 9. Temperature dependence of the effective energy of hexagonal anisotropy ω_q. Dots correspond to experimental data [14, 33, 51].

on $FeBO_3$ crystals in [51] grown under different conditions have shown rather good agreement with the results of measurements of different samples in the temperature range 30–300 K and gave grounds to assume that the observed anisotropy is by no means due to the impurity ions (later, this assumption was confirmed by the results of calculations [14, 32, 34]). On the contrary, the measurements performed on different crystals at low temperatures (1.5–10 K) have shown a significant spread of the values of resonance fields.

In the temperature range 5–7 K, a compensation point of hexagonal anisotropy was revealed, at which a spin-reorientation phase transition occurs. Figure 9 shows the temperature dependence of the effective energy of hexagonal anisotropy in the $FeBO_3$ crystal [14, 51].

The above results indicate that in crystals of ferric borate synthesized by the methods used in [14, 51], there are impurities that significantly affect the linewidth and the basal anisotropy at low temperatures. At the point of compensation and in its vicinity, an anomalous behavior of the linewidth and a hysteresis of the resonance field are observed.

2.5 Anisotropic interactions in paramagnetic and magnetically ordered dielectrics with S ions

In this section, we compare the results of calculations of the temperature dependence of the anisotropy of magnetically concentrated crystals with experimental data.

2.5.1 Anisotropy constants of spin Hamiltonians of isolated ions. Table 1 contains the values of the spin Hamiltonian constants that are determined by the EPR method from the dependences of the lattice parameters of diamagnetic analogs corresponding to iron borate, manganese carbonate, hematite, $(CH_3)_4NMnCl_3$, MnF_2, $Y_3Fe_5O_{12}$ (cubic unit cell is given in [52]), and EuO (Nal-type structure [37]).

2.5.2 Anisotropy constants of spin Hamiltonians of paired ions. In passing from the description of isolated ions to the description of pairs of ions, the physical picture of the interactions becomes significantly more complex.

In view of the increase in the number of particles in the system, the Heisenberg invariant of the isotropic exchange energy is now introduced. The Hamiltonian for a pair of ions has been obtained in terms of the total spin in [49], and in terms of spins of isolated ions (with additional anisotropic exchange terms), in [2]. In [15], a qualitatively different physical picture is considered, according to which the 'single-ion' anisotropy appears as a result of covalent effects. Such a variant of interactions has been calculated in theoretical study [44], where a conclusion was made on an analogous contribution (in terms of the operator structure [2]) of these processes to the 'single-ion' exchange anisotropy.

In the diamagnetic analogs with an impurity of paired paramagnetic ions, the axial constant of spin Hamiltonian (8), $D_{cS}(S) = D_{cf} + D_{c0} + A\sqrt{S(S+1)}$, is proportional to the exchange field $H^{ex} = (J/g\mu_B)\sqrt{S(S+1)}$ at the multiplets of the pair. The fourth-order constant $(a-F)_{cS}$ of the spin Hamiltonian has not been obtained in the approximation under consideration [2, 44]. It is assumed (in particular, based on experimental data obtained on pairs of Fe^{3+} ions in MBO_3) that $(a-F)_{cS} \sim (H^{ex})^2$ for different multiplets of this compound. It can be seen from Fig. 5 and the expression for $D_{cS}(S)$ that for $MBO_3 + Fe^{3+}$ compounds, the axial 'single-ion' constants of the spin Hamiltonian of the second and fourth orders (D_{cS} and $(a-F)_{cS}$) are described well by the approximate dependences $\sim\sqrt{S(S+1)}$ and $S(S+1)$. The fitting parameters A and B, which describe the 'single-ion' contributions in the system of $MBO_3 + Fe^{3+}$ crystals, are respectively proportional to c_H/a_H and $(c_H/a_H)^2$ (see Figs 6 and 7). In Figure 10 [47] (see also [53]), the exchange-dependent contribution to the 'single-ion' constant of the pair can be seen well. Extrapolating the dependence shown in Fig. 10 to the zero exchange field at the multiplets of the pair shows that the parameter D_{cS} should be equal to the constant of the spin Hamiltonian of an isolated ion plus the D_{c0} contribution due to the distortion of the lattice by the 'foreign' pair.

As can be seen from Figure 11 [15], the 'single-ion' exchange fields of the axial anisotropy constants that

Table 1. Values of the constants of the spin Hamiltonians of isolated ions determined using diamagnetic analogs corresponding to magnetically concentrated crystals (in the magnitudes of lattice parameters)*.

Compound	D_{cfmc}, Oe	$(a-F)_{cfmc}$, Oe	a_{cfmc}, Oe	F_{cfmc}, Oe	α_{cfmc}, deg	a_{acfmc}, Oe	a_{dcfmc}, Oe	F_{acfmc}, Oe	F_{dcfmc}, Oe
$FeBO_3$	1005 ± 12	189.3 ± 9	132 ± 20	-56.7 ± 20	24 ± 2				
$MnCO_3$	25 [16]	−13.0 [16]							
α-Fe_2O_3	1797	209.7							
EuO			−2.2						
$Y_3Fe_5O_{12}$						272.5	65.4	135.8	0.8
$(CH_3)_4NMnCl_3$	43.9 [23]								
MnF_2	−133								

* D_{cfmc}, $(a-F)_{cfmc}$, a_{cfmc}, F_{cfmc}, and α_{cfmc} are the constants of Hamiltonian (3) (see also Fig. 1); a_{acfmc}, F_{acfmc} and a_{dcfmc}, F_{dcfmc} are the cubic and axial constants of the spin Hamiltonian in octahedral and tetrahedral positions of the garnet lattice.

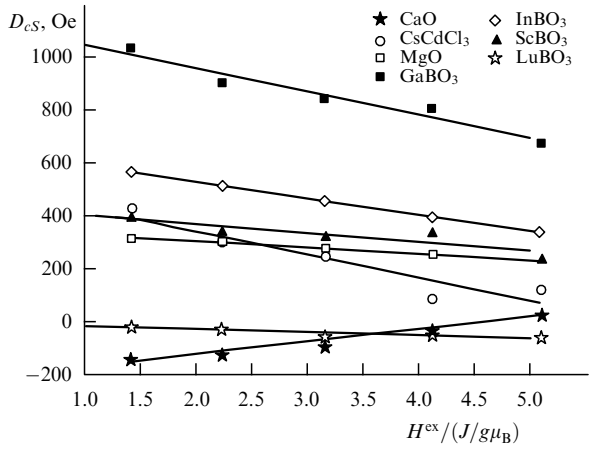

Figure 10. Dependence of the 'single-ion' constants D_{cS} of the spin Hamiltonian of the antiferromagnetically coupled ions $Mn^{2+}-Mn^{2+}$ and $Fe^{3+}-Fe^{3+}$ in CaO, $CsCdCl_3$, MgO, and MBO_3 (M = Ga, In, Sc, Lu) crystals on the exchange field $H^{ex}/(J/g\mu_B) = [S(S+1)]^{1/2}$ [47]. J is the exchange parameter; g is the spectroscopic splitting factor.

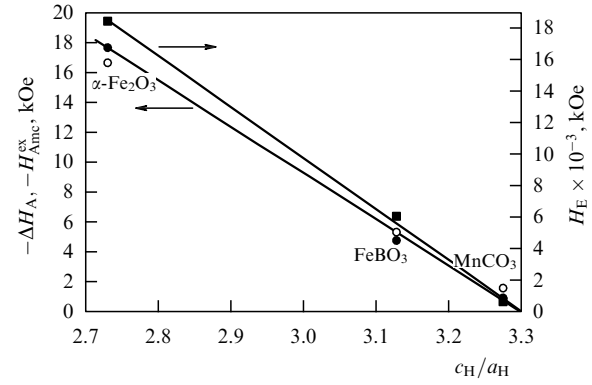

Figure 11. Dependence of the exchange fields H_E (squares) and ΔH_A (deviations of the calculated single-ion and dipole contributions from the experimental values, solid circles) in manganese carbonate, iron borate, and hematite on the ratio of the lattice parameters of the hexagonal lattice at $T = 0$. The white dots correspond to the contribution of the 'single-ion' exchange anisotropy field H^{ex}_{Amc}.

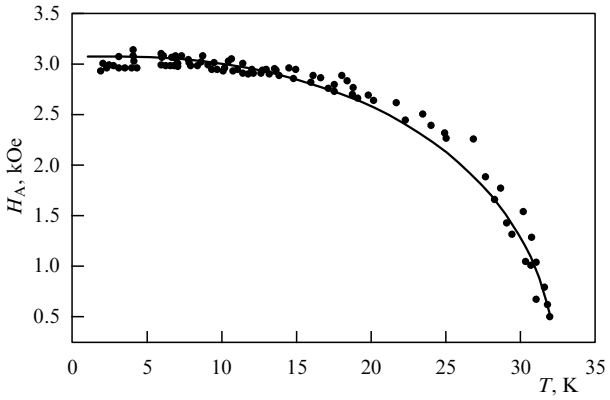

Figure 12. Temperature dependence of the uniaxial anisotropy field H_A in manganese carbonate. The dots denote experimental data [54]; the solid line corresponds to the calculated results [45].

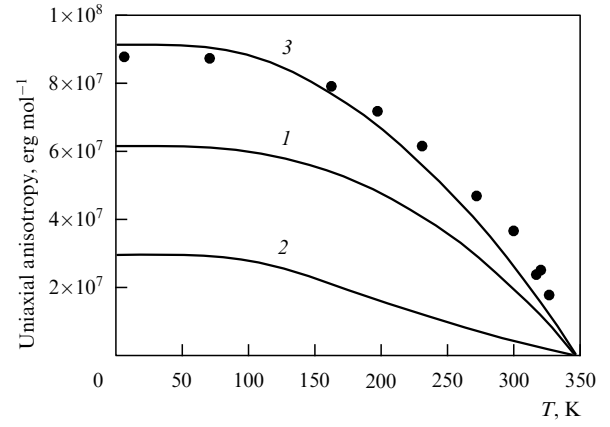

Figure 13. Temperature dependence of the uniaxial anisotropy constants $a(Fe^{3+})$, $a'(Fe^{2+})$, and $a(Fe^{3+}) + a'(Fe^{2+})$ in iron borate. Dots denote experimental data [57, 58]; the solid lines correspond to the calculated results [33]. Curve *1* corresponds to the contribution from Fe^{3+} ions; curve *2* is the contribution from Fe^{2+} ions; curve *3* is the sum of the contributions from the ions of divalent and tervalent iron.

describe magnetically concentrated compounds with S-state ions also depend on the isotropic exchange field linearly.

2.5.3 Uniaxial and hexagonal anisotropy of rhombohedral antiferromagnetic crystals. Temperature dependence. Figure 12 shows the temperature dependence of the uniaxial anisotropy field H_A of $MnCO_3$ crystals [45]. In calculating H_A from the products of the exchange field and anisotropy field, the results of experimental studies [36, 54–56] have been used. The least-square fitting of the data was performed with the use of the dependences of two mechanisms, dipole and 'single-ion'. One fitting parameter ($D'_c = -0.75$ kOe, see Section 2.3.5) and one fixed parameter, the calculated anisotropy field ($A'_{dip} = H_{Adip}(0) = 3.82$ kOe), were used. According to the EPR data, the magnitude of D'_c (which includes the contributions from isolated ions and paired ions of the 'single-ion' mechanism) is -0.98 kOe.

Figure 13 demonstrates the temperature dependence of the uniaxial anisotropy constants of $FeBO_3$ crystals with an Fe^{2+} impurity [33] in comparison with the experimental data [57, 58]. The fitting was done together with the fitting of the temperature dependence of the hexagonal anisotropy (see Fig. 9). Two fitting parameters and four fixed parameters were used. As the fitting parameters, the uniaxial anisotropy constant $c_0 A_2^0 = 9.87 \times 10^{-18}$ erg ion, which is controlled by Fe^{2+} ions, and the parameter $c_0 B_{imp} = 1.125 \times 10^{-52}$ erg^3 ion, which also is controlled by Fe^{2+} ions, were taken. The fixed parameters were the dipole interaction constants; two 'single-ion' constants in the terms of the second (D'_c) and fourth (E'_c) order, which are obtained from the EPR data, and the hexagonal anisotropy constant found by extrapolating the Fe^{3+} contribution from $T = 77$ K to $T = 0$, which is equal to -0.011 Oe (-3.1×10^2 erg mol^{-1}). The quantity $A'_{dip} = H_{Adip}(0)$ is equal to 3.66 kOe (10.25×10^7 erg mol^{-1}) [14, 27, 59]. According to the EPR data, the quantities D'_c and E'_c, whose sum is the (constant) anisotropy field caused by the 'single-ion' contribution from Fe^{3+}, at $T = 0$ are respectively equal to -0.84 kOe (-2.35×10^7 erg mol^{-1}) and -0.20 kOe (-0.56×10^7 erg mol^{-1}).

To describe the temperature dependence of the first and second anisotropy constants in hematite, it is necessary to use five fitting parameters and one fixed parameter (the magni-

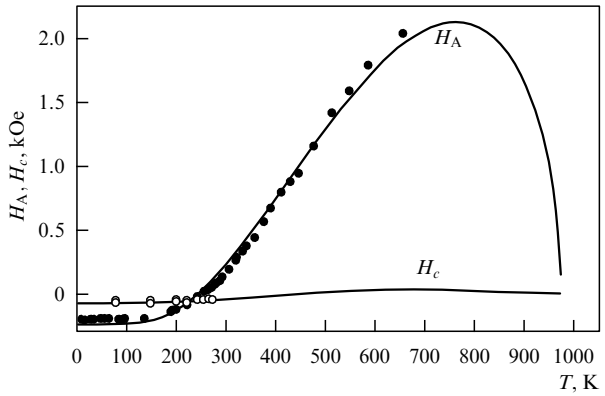

Figure 14. Temperature dependence of the uniaxial anisotropy fields of the first (H_A) and second (H_c) constants in hematite. The dots denote experimental data [60, 61]; the solid lines correspond to the calculated results [45].

tude of the dipole contribution). The second constant can be measured only at temperatures that do not exceed the Morin temperature, i.e., only in the antiferromagnetic phase [60, 61]. The experimental temperature dependences of the anisotropy fields of the first and second constants for hematite are given in [60] and [61].

The simultaneous least-square fitting of the effective fields of the first and second anisotropy constants gives $A'_{ex} = 3.20$, $D'_c = -12.57$, $C'_{ex} = 2.64$, $E'_c = -0.97$, and $B'_{ex} = -2.58$ kOe (see Section 2.3.5). The fitting results are shown in Fig. 14.

The insufficiently exact Néel temperature for hematite, the use of the Brillouin function instead of the magnetizations of the sublattices, and the relatively large number of fitting parameters exert a negative effect on the precision of the quantitative estimates of the anisotropy for these crystals.

2.6 Sources of uniaxial and hexagonal anisotropy in magnetically concentrated crystals with S-state ions. Generalized independent method of proper quantitative description of magnetic anisotropy

Table 2 contains the experimental values of the anisotropy fields in S-state ions in magnetically concentrated crystals and the fields determined from the data for the diamagnetic analogs by the EPR method.

It can be seen from Table 2 that taking the 'single-ion' exchange anisotropy into account along with other contributions leads to a satisfactory agreement with the experimental results. For the $YFe_3(BO_3)_4$ compound, no EPR data for diamagnetic analogs exist; therefore, a corresponding estimation is impossible. However, because the temperature dependence of the uniaxial anisotropy constant is described well by the Brillouin function [3, 4], it is the dipole contribution that dominates. The single-ion and 'single-ion' exchange contributions compensate each other. For H_A in $FeBO_3$, Table 2 gives the values only due to Fe^{3+} ions.

Using the above results, we can formulate a generalized method of a proper quantitative description and prediction of the anisotropy of magnetically ordered crystals with S-state ions. The basis for such a generalization is the fact that both single-ion and 'single-ion' exchange mechanisms are characterized by the same temperature dependence of magnetic anisotropy [13, 29, 33].

The method includes [33, 53], first, the investigation of magnetic anisotropy of an impurity-free system of the crystal (calculation of the contribution from dipole interactions, estimation of the single-ion contribution by the EPR method in isostructural diamagnetic analogs with an impurity of ions of a magnetically concentrated substance, and estimation of the 'single-ion' exchange anisotropy using EPR spectra of pairs of paramagnetic ions in a series of diamagnetic analogs) and, second, the calculation of the effect of an impurity (if present) on the magnetic anisotropy.

The complete direct estimation of the contributions to the hexagonal anisotropy of $FeBO_3$ and to the cubic anisotropy of EuO and $Y_3Fe_5O_{12}$ cannot be performed to date because of the absence of independent experimental and theoretical results. However, it follows indirectly from the general picture of the interactions and available experimental data (in particular, concerning the temperature dependences) that the 'single-ion' exchange mechanism should also make a contribution to this anisotropy and correctly describe the experimental quantitative data.

The experimental value of the effective hexagonal anisotropy energy (field) extrapolated from $T = 7$ K to $T = 0$ K is $\omega_q(Fe^{3+}) = -3.1 \times 10^2$ erg mol^{-1} ($H_q = -0.011$ Oe) [14, 32]. The theoretical value of this energy caused by the interaction of ion spins with the crystal field is $\omega_{q\text{cfmc}}(Fe^{3+}) = -5.3 \times 10^2$ erg mol^{-1} ($H_{q\text{cfmc}} = -0.019$ Oe).

One of the hexagonal anisotropy mechanisms is the coupling between the spin (not less than 2) with the cubic electric field of the crystal. This coupling is manifested in that the magnetic moments of the ions deviate from the nearest cubic axes (or become inclined toward them) (see Fig. 1) and therefore periodically leave the basal plane of the crystal upon their rotation about the c_3 axis. Because of the misorientation

Table 2. Effective anisotropy fields* in magnetically concentrated crystals at $T = 0$ K.

Compound	$H_{A\text{cfmc}}$, kOe	$H_{A\text{dip}}$, kOe	$H^{ex}_{A\text{mc}}$, kOe	ΔH_A, kOe	H_A, kOe	$H_{A\text{Tmc}}$, kOe
$Y_3Fe_5O_{12}$	−0.25	0		0.12	−0.13 [29]	
EuO	0.01	0		−0.24	−0.23 [13]	
MnF_2	−0.53 [62]	−8.37 [62]		0.88	−8.02 [62]	
$(CH_3)_4NMnCl_3$	0.18 [53]	6.77 [63]	−2.02		4.16; 4.89; 5.95 [63]	4.93
$FeBO_3(Fe^{3+})$	4.21 ± 0.05 [31, 33]	3.66 ± 1% [14, 27, 59]	−5.25 ± 0.1 [33]	−5.67 ± 0.1	2.20 [31]	2.62 ± 0.2 [33]
$MnCO_3$	0.090 [16]	3.82 [27]	−1.04 [15, 16, 33, 48]	−0.90 [33]	3.01 [54]	2.87 [16]
α-Fe_2O_3	7.94 [15, 48]	10.04 [28]	−16.28 [15, 48]	−18.20 [15, 48]	−0.22 [58, 59]	1.69 [15, 48]

* $H_{A\text{cfmc}}$ is the single-ion field of the crystal calculated based on EPR data; $H_{A\text{dip}}$ is the calculated dipole anisotropy field in a magnetically concentrated crystal; $H^{ex}_{A\text{mc}}$ is the 'single-ion' exchange field calculated using the EPR data for pairs of ions; H_A is the experimental value of the anisotropy field in a magnetically concentrated crystal; $H_{A\text{Tmc}}$ is the theoretical value of the anisotropy field (the sum of contributions from the mechanisms that are taken into account in this paper) in a magnetically concentrated crystal; $\Delta H_A = H_A - H_{A\text{cfmc}} - H_{A\text{dip}} \approx H^{ex}_{A\text{mc}}$.

of the cubic axes ξ_1, η_1, ζ_1 and ξ_2, η_2, ζ_2 (see Fig. 1) and due to the antiferromagnetic ordering of the sublattice moments, the maximum deviations of the vector **l** are possible at the angles $\varphi = \pi n/3$, $n = 0, 1, 2, \ldots$ [32]. These conclusions are in agreement with the phenomenological theory [9, 10].

Although the origin of the Dzyaloshinskii–Moriya interaction $\mathbf{D}_{12}[\mathbf{s}_1 \times \mathbf{s}_2]$ in rhombohedral crystals has long been clarified (antisymmetric anisotropic exchange [64]), the method for determining the sign of $\mathbf{D}_{12}$ was developed only recently [65]. In [65], the $FeBO_3$ crystal was taken as the sample for the analysis (two nonequivalent positions are shown in Fig. 1). The crystal could rotate in the (111) plane (in the rhombohedral setting) through an angle ψ about the c_3 axis. The rotation of the vector of the constant magnetic field acting on the crystal (which also lay in the (111) plane) was specified by the angle η. The angles ψ and η were counted from the twofold axis of the crystal.

The standard method for determining the magnetic structure — neutron diffraction — does not make it possible to determine the sign of the deviation of spins, which is specified by the phase of the wave that interacts with the crystal because of the low intensity of the wave. The new method presented in [65] is based on the interference between the resonance synchrotron scattering and magnetic scattering. Resonance scattering processes are controlled by electric phenomena. It turns out that the signals of both resonance and magnetic scattering are observed at the same positions of Bragg reflections. These signals have comparable amplitudes, which increase due to the interference effects. The sign and amplitude of the magnetic scattering signal depend on the direction of spins, which can be changed by rotating the magnetic field vector in the crystal, whereas the resonance scattering depends on the energy of the wave and orientation of the crystal. The magnetic scattering phase can be determined by controlling both these processes.

Figure 15 shows the shift of the resonance scattering peak when rotating through the angle $\eta = 180°$. An opposite shift was observed when the resonance scattering phase was changed by rotation through the angle ψ. The processing of experimental data allowed determining the sign of the Dzyaloshinskii–Moriya vector, the phase and amplitude of magnetic scattering, and the direction of the shift. The sign of the Dzyaloshinskii–Moriya interaction in the $FeBO_3$ crystal proved to be negative.

The authors of [65] also performed *ab initio* calculations using the local density approximation (LDA) method with the electrostatic Coulomb and spin–orbit interactions. The calculated vector $\mathbf{D}_{12} = (-0.25 \text{ meV}, 0, -0.24 \text{ meV})$ lies in the XZ plane (in [65], $X \| c_2$ is parallel to the c_2 axis of the crystal, and the external magnetic field **H** is parallel to Y, which differs from the directions of the crystal axes and the direction of the field **H** shown in Fig. 1). The calculated angle of the sublattice angularity is 0.7°, and the experimental angle is 0.9°. All six symmetrically equivalent vectors have identical Z components, whereas the XY components give zero upon summation.

3. Multiferroic bismuth ferrite. Possibilities of the uniaxial anisotropy investigation (with the use of a diamagnetic analog with an Fe^{3+} impurity) in the parameter region of the spin cycloid existence in $BiFeO_3$

The $BiFeO_3$ Seignette magnet, which exhibits magnetic and electric ordering simultaneously, has been investigated in numerous studies (see, e.g., [7] and the references therein). The intensive growth of the number of publications in recent years is related to the possibility of creating various unique devices based on $BiFeO_3$ [8]. The possibilities of applications of $BiFeO_3$ are determined to a significant extent by the existence of magnetic and electric moments in it.

Multiferroic bismuth ferrite has the electric ordering temperature $T_C = 1083$ K [6]. At the Curie temperature T_C, $BiFeO_3$ goes from the cubic perovskite phase into a rhombohedrally distorted phase (with the unit cell doubled along the c_3 axis because of the antiparallel rotation of oxygen octahedra about the [111] direction), which belongs to the space group $R3c$ [8]. The magnetic ordering occurs at temperatures below the Néel temperature $T_N = 643$ K [6].

Recent neutron diffraction studies [66] have revealed a complex spatially modulated structure with a large period in $BiFeO_3$. The magnetic moments of Fe^{3+} ions, retaining the mutual local antiferromagnetic orientation, become arranged along the propagation direction (one of the twofold axes) of

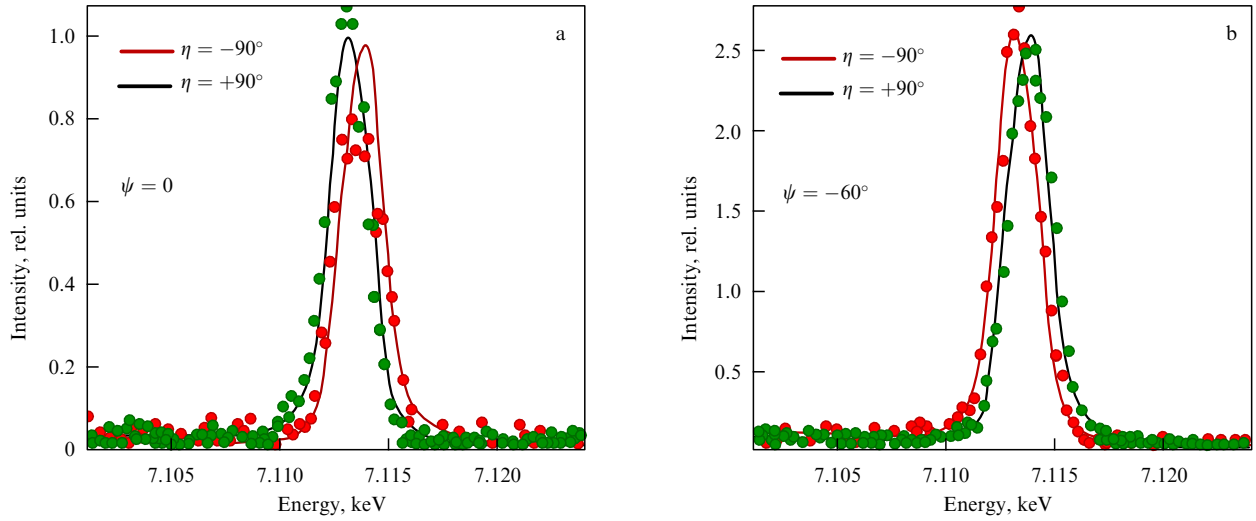

Figure 15. (In color online) (a) Shifts of the resonance peaks of synchrotron radiation upon rotating the constant magnetic field through the angle $\eta = \pm 90°$ in the basal plane of the $FeBO_3$ crystal. (b) The opposite shifts at $\eta = \pm 90°$ and $\psi = -60°$.

the modulated wave in the plane perpendicular to [111] [6] (a schematic of the cycloid is given, e.g., in [6, 8]). The average magnetic moment is then equal to zero, which makes it impossible to efficiently control the electric properties via magnetic actions and vice versa [8]. The nonzero magnetic moment in $BiFeO_3$ (which is determined by the Dzyaloshinskii–Moriya interaction) appears upon the suppression of the cycloid, e.g., in an external magnetic field of about 180 kOe [8].

The magnetic anisotropy plays a significant role in the formation of the region of existence of a spin cycloid and of the critical field for its disappearance [8]. The critical field calculated in [6] in the approximation of a harmonic cycloid is given by

$$H_c = \sqrt{\frac{2(K + 2Aq^2)}{\chi}},$$

where H_c is the external critical field oriented along the threefold axis, K is the uniaxial magnetocrystalline anisotropy constant, A is the inhomogeneous exchange constant, q is the magnitude of the wave vector of spin modulation of the cycloid corresponding to the free-energy minimum, and χ is the susceptibility in the direction perpendicular to the antiferromagnetism vector. The free energy that was used to derive this expression is given in [6].

The phase diagram that describes the regions of the existence of a spatially modulated spin structure is shown in Fig. 16 [8]. The expression for the free energy whose minimization was used to derive this phase diagram is given in [8].

The magnitude of the electric polarization in $BiFeO_3$ depends on the applied magnetic field [6]. The varying polarization leads to a change in the internal electric field, which causes Stark splitting of the levels of magnetic ions. This leads to a change in the spin–orbit interaction and, as a result, to a change in the energy of single-ion anisotropy [67, 68] and in the 'single-ion' exchange anisotropy. Consequently, the magnetic anisotropy in these crystals should depend on the magnitude of the applied magnetic field.

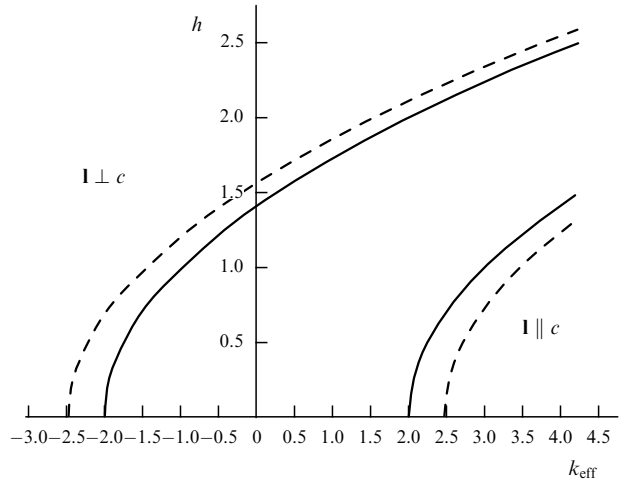

Figure 16. Phase diagram for $BiFeO_3$ [8] constructed in the coordinates "reduced external magnetic field–effective uniaxial anisotropy constant." Here, c is the threefold axis, $h = H[\chi/(2Aq^2)]^{1/2}$ is the reduced energy of the external magnetic field, $k_{eff} = [K/(Aq^2)] - [M_s^2/(2Aq^2\chi)]$ is the effective uniaxial anisotropy constant, which includes the reduced energies of uniaxial anisotropy and Dzyaloshinskii–Moriya interaction, and M_s is a weakly ferromagnetic moment. The solid lines are the boundaries between the homogeneous antiferromagnetic state and the spatially modulated spin structure calculated in the harmonic approximation of the cycloid; the dashed lines are the same boundaries calculated in the anharmonic approximation.

Because the magnetic anisotropy of $BiFeO_3$ in the region of the existence of the cycloid (in weak and middle fields) cannot be studied by the AFMR method [8], it can be estimated using a ferroelectric diamagnetic analog, e.g., $BiAlO_3$ (axial ratio of the hexagonal unit cell $c_H/a_H = 2.49$ [69], $T_C \approx 520\,^{\circ}C$ [70]). For $BiFeO_3$, $c_H/a_H = 2.42$ [71]. The X-ray diffraction parameters of the deviations of the positions of iron and oxygen ions in the unit cell of these compounds from those characteristic of the space group $R3c$ are also close to one another [69].

4. Anisotropic interactions and nanostructures. Skyrmions

The fundamental character of anisotropic interaction manifests itself not only in 'conventional' crystals but also in crystals with nanostructures, for example, as skyrmions in thin magnetic films (several atomic layers thick).

It has been shown in [72] that the electric field applied to a film with the structure MgO (001) substrate/MgO (10 nm)/Cr (10 nm)/Au (50 nm)/Fe (2–4 atomic layers)/MgO (10 nm)/polyamide (1500 nm) can lead to large changes (about 40% of the magnetic anisotropy magnitude) in Fe/MgO contacts, which significantly exceeds the changes in the magnetic anisotropy obtained previously under different experimental conditions (different materials and different fabrication technology).

The total anisotropy of the film is composed of the change in the anisotropy caused by the energy of the demagnetizing field, magnetocrystalline anisotropy, the surface anisotropy of the Fe/MgO and Fe/Au interfaces, and the anisotropy change due to the applied electric field. The electric field was applied to the layers of polyamide (positive) and Au (negative); as a result, the energy of the total magnetic anisotropy changed, which led to a reorientation of the magnetization. The change in the anisotropy apparently occurs because of the change in the electron population of 3d orbitals of iron adjacent to the MgO barrier in the magnetizing field perpendicular to the film surface [72].

Switching over the magnetization in tunnel contacts can be used, for example, in developing low-power logical devices and energy-independent memory cells.

One more interesting phenomenon caused by the Dzyaloshinskii–Moriya interaction is skyrmions, which are spin vortices about 20–100 nm in size. Skyrmions form an ordered two-dimensional lattice in substances such as single-crystal metallic compounds (MnSi) [73], strongly correlated metals ($Fe_{0.5}Co_{0.5}Si$) [74], and some dielectrics (Cu_2SeO_3) [75].

The possibility of the existence of skyrmions was predicted theoretically by Bogdanov and Yablonskii [76]. They drew an analogy, in particular, with superconductors, in which inhomogeneous stable states can exist in the region of a first-order phase transition induced by an external magnetic field. It was shown theoretically that in magnets of some symmetry in a certain range of external magnetic fields, stable vortex formations analogous to states in superconductors can appear. The skyrmions arise under conditions of a helicoidal magnetic order upon the application of a constant external magnetic field in a certain range of temperatures.

An important parameter in the description of vortices is the topological index [77]

$$S = \frac{1}{4\pi} \int \mathbf{n} \left[\frac{\partial \mathbf{n}}{\partial x} \times \frac{\partial \mathbf{n}}{\partial y} \right] \mathrm{d}x\, \mathrm{d}y\,,$$

where **n** is the unit vector of the local magnetization and the integral is taken over the two-dimensional unit cell. For compounds such as ferromagnets and antiferromagnets, $S = 0$. If $S = \pm 1$, then a topologically stable knot exists in the spatial distribution of the magnetization.

In this review, we mainly consider studies concerning the investigation of skyrmions for two limit compounds (in terms of conductivity): a metallic compound MnSi and a dielectric compound Cu_2OSeO_3 (which is a multiferroic). These compounds crystallize into a *B20* cubic structure with a shifted symmetry center. The unit cell of MnSi [78] is shown in Figs 17a, 17b; the crystal structure of Cu_2OSeO_3 is depicted in Fig. 17c; the magnetic structure of Cu_2OSeO_3 is given in Fig. 17d.

Skyrmions could not be revealed experimentally for a long time. It is only in 2009 that a new magnetic phase was revealed that was interpreted as a lattice of skyrmions. Notably, the neutron diffraction data have shown the existence of magnetic Bragg peaks of hexagonal symmetry compatible with the superposition of three helicoids oriented at angles of 120°. These helicoids lie in the plane perpendicular to the applied magnetic field. A theoretical analysis in [73] in terms of the Ginzburg–Landau model confirmed the existence of a lattice of skyrmions that form the so-called A phase. However, according to the experimental data [73], this spin structure in reality can represent either a lattice of skyrmions or a superposition of helices. Neutron diffraction experiments cannot resolve this question [79].

The existence of skyrmions in the form of separate spin structures can be confirmed using topological Hall effect measurements [79]. The source of the topological Hall effect is the Berry phase caused by concentrated conduction electrons on the background of a strongly inhomogeneous magnetic state of the skyrmion lattice [79]. The topological Hall effect arises along with the normal Hall effect, which is

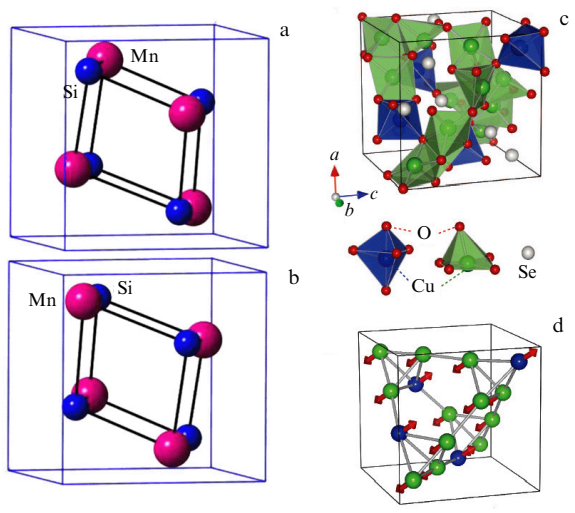

Figure 17. Crystal structure of (a) right-hand and (b) left-hand forms of MnSi [78]. (c) Crystal structure of Cu_2OSeO_3 characterized by two nonequivalent positions of Cu^{2+} ions with different oxygen surroundings. (d) Ferrimagnetic spin arrangement of copper ions [75].

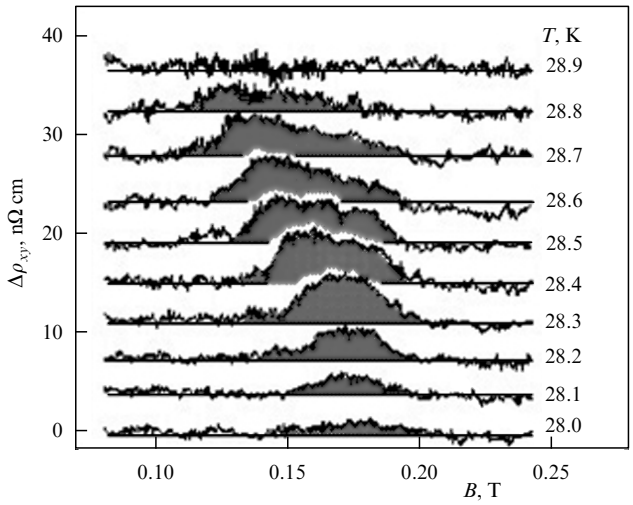

Figure 18. Additional contribution to the resistance, $\Delta\rho_{xy}$, caused by the topological Hall effect in the MnSi crystal [79]. The magnetic field and the current are parallel to the respective directions [110] and [001].

proportional to the applied magnetic field. The topological Hall effect is related to the ferromagnetic components of the magnetization [79]. Figure 18 shows the dependence of the resistance caused by the contribution from the topological Hall effect on the applied induction B in the MnSi crystal at different temperatures (the vector of current is parallel to [001]; the induction vector is parallel to [110]). This dependence demonstrates the existence of skyrmions in the region of the A phase.

The above-described methods are not visual. The direct observation of skyrmions was first performed using Lorentz electron microscopy on $Fe_{0.5}Co_{0.5}Si$ in [74]. A photo of skyrmions [75] obtained using a Lorentz microscope for a thin film of Cu_2OSeO_3 is shown in Fig. 19a; Fig. 19b illustrates a model of skyrmions. Previously, the Lorentz microscopy was used to observe domain walls in ferromagnetic films. The domain walls are not seen in the focused mode in the electron microscope; they become visible as black or white regions only if the microscope is defocused. Upon passing through neighboring domains, two electron beams are reflected in different directions in such a way that the two beams overlap or become separated and, thus, the intensity increases or decreases along the domain wall [80].

Because the MnSi compound is metallic, the first investigations of its properties were performed based on the energy band theory. In [81], a phase diagram (Fig. 20) constructed based on the experimental data for MnSi available in the literature is shown. This diagram was interpreted and the properties of manganese silicide were explained in terms of the energy band theory. In the magnetic field $H = 0$ at $T = 29$ K, the spins, according to this diagram, begin ordering helically with a period of 18 nm. At temperatures below T_C, an increase in H to ~ 1 kOe leads to a transition from the helical order to a conical state, and at $H \sim 6$ kOe, to a ferromagnetic state. The skyrmion phase is observed in a narrow region of temperatures and fields.

However, in recent years MnSi is again attracting the attention of researchers in view of the problem of helicoidal states, skyrmions [81], and contradictions with the energy band model that was used initially for the description of experimental data. In particular, it was noted in [81] that,

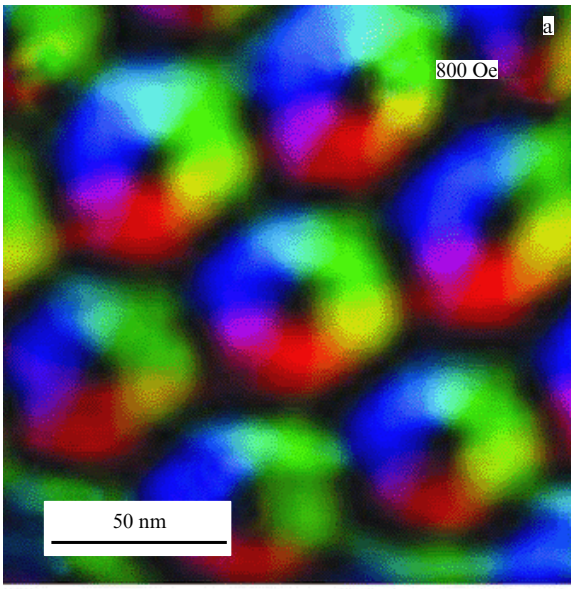

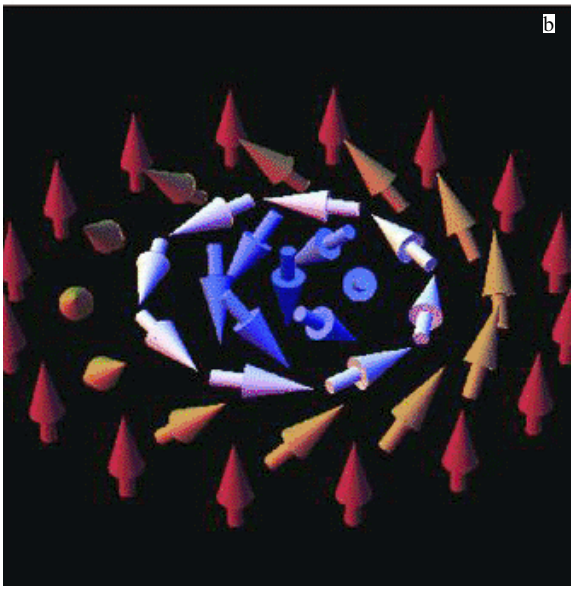

Figure 19. (a) Photo of skyrmions in a thin magnetic film of Cu_2OSeO_3 at $T = 5$ K in the (111) plane (obtained by Lorentz microscopy). (b) Model of a skyrmion [75].

first, the skyrmions are localized spin 'particles' [76]; second, according to LDA calculations [81, 82], the spin density, whose magnitude is independent of the external field up to ~ 1000 kOe, is concentrated mainly in the Mn ion; in the Si atom, it composes only 2–3% of the magnetic moment of Mn; and, third, experimental data on the high-frequency dynamic conductivity of MnSi contradict the model of the weak itinerant-electron magnet.

We note that according to the recent data in [83], the crossover between the paramagnetic (PM) and spin-polarized (SP) phases is absent (see Fig. 20). The regions of the PM phase and SP phase are separated by a vertical straight line $T = T_C$.

From the microscopic standpoint, the nature of the magnetic moments that form the skyrmion states in MnSi is unclear. On the one hand, the theory in [76] suggests the existence of localized magnetic moments (LMMs), and

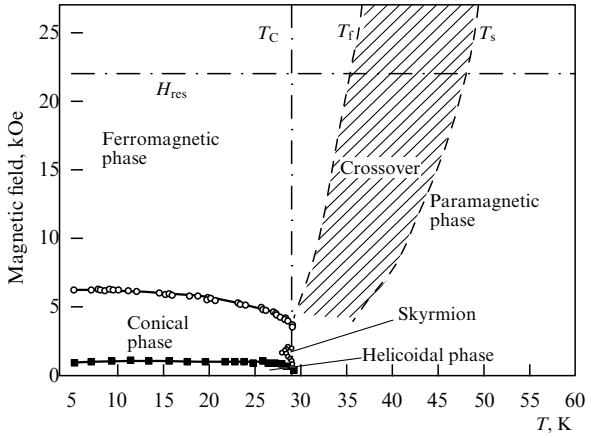

Figure 20. Magnetic phase diagram of MnSi. Regions are indicated that correspond to the helicoidal, conical, skyrmionic, ferromagnetic, and paramagnetic phases; the crossover region is hatched. H_{res} is the field of magnetic resonance in the EPR experiment; T_s and T_f are the temperatures that determine the width of the crossover on the level of the field of paramagnetic resonance [81].

almost all experiments are interpreted in terms of this concept. On the other hand, MnSi is a conducting material, and it is precisely MnSi that was considered an example of a weak band (itinerant-electron) ferromagnet with strong spin fluctuations [84]. The band theory [85] gives a spin moment in the Mn ion equal to about μ_B. The experimentally observed dependence of the Curie–Weiss paramagnetic susceptibility at temperatures above T_C agrees with the spin-fluctuation theory [84], and the calculated effective magnetic moment is close to that observed at temperatures above T_C. However, in the range of temperatures below T_C, the measured magnetic moment ($0.30\,\mu_B$ per Mn ion) does not agree with the results of band theory calculations, which do not take quantum spin fluctuations into account. At the same time, spin relaxation in the system of LMMs in MnSi, which determines the EPR line width, is described in terms of the Moriya spin-fluctuation theory [81]. Thus, using the example of MnSi, we see the manifestation of the classical dualism of the magnetism of 3d electron systems: some properties can be described in the model of LMMs, but the description of others requires itinerant electrons.

The authors of [81] have studied the EPR on MnSi crystals (at a frequency of 60 GHz) in the temperature range 4.2–300 K in external magnetic fields up to 70 kOe. The results of the EPR measurements were explained based on the spin-polaron model, which previously proved to be efficient for describing the magnetic properties of FeSi [81, 86]. According to this model, it is assumed that antiferromagnetically ordered band carriers are formed around ferromagnetically localized magnetic moments. It follows from the EPR measurements that the resonance field H_{res} is constant in the entire temperature range (see Fig. 20); the g factor in this case is equal to approximately 2, which suggests that the wave function of the localized spin moments of the positively polarized charge carriers has an S-like shape.

The sources of helicoidal and conical states in MnSi (which are responsible for the formation of skyrmions) were considered in [87] based on the Heisenberg Hamiltonian

$$\hat{H}_0 = \frac{1}{2}\sum_{i,j}\left(-J\mathbf{s}_i\,\mathbf{s}_j + \mathbf{D}_{ij}[\mathbf{s}_i \times \mathbf{s}_j]\right) - g\mu_B\sum_i \mathbf{H}\mathbf{s}_i\,, \qquad (16)$$

where the first term in the parentheses describes the isotropic exchange interaction, the second term corresponds to the Dzyaloshinskii–Moriya interaction, and the last term describes the interaction of spins with the external magnetic field. The summation over the index i ranges all ions of the crystal; the summation over j ranges the nearest neighbors of the ions i.

The energy under the condition $g\mu_B H \sim D^2/J$ can be written as

$$E = NJ\left[-12 - 2\frac{(D_x + D_z)^2}{J^2} - \frac{1}{3}\frac{(D_x - 2D_y - D_z)^2}{J^2} - 12\frac{(g\mu_B H)^2}{(D_x - 2D_y - D_z)^2}\right], \quad (17)$$

where N is the number of unit cells in the crystal. The first term in the brackets describes the isotropic exchange energy, the second term is the energy responsible for the deviation from the ferromagnetic order, the third term is the 'twisting' of the ferromagnetism vector (within the interaction of the unit-cell ions with the nearest neighbors if $N = 1$) characteristic of the helicoidal structure, and the last term describes the effect of the external magnetic field. When the external magnetic field H_{ext} exceeds the critical value $H_c = (D_x - 2D_y - D_z)/(6Jg\mu_B)$, the helicoid passes into the conical phase. Here, the magnetic field is oriented along the c_3 axis and coincides with the orientation of the wave vector.

In bulk samples, skyrmions exist only in narrow ranges of fields and temperatures. It was shown in [88] that the easy-plane uniaxial anisotropy substantially extends the region of existence of skyrmions. In particular, the effect of this anisotropy is observed in films. Figure 21 displays the phase diagram in the "applied magnetic field–temperature" coordinates for the bulk and film samples of ferrimagnetic magnetoelectric Cu_2OSeO_3 [75]. The magnetic structure of Cu_2OSeO_3 is given in [75]; $T_C = 60$ K. The magnetic period of the helicoid modulation is 63 nm [88], which is much greater than the lattice parameter (0.89 nm). Skyrmions in Cu_2OSeO_3 have recently been observed by Lorentz TEM [75] and small-angle neutron spectroscopy [90, 91]. In dielectrics, skyrmions can be manipulated by external electric fields, rather than by currents, as in metals and semiconductors, thereby avoiding ohmic losses. Such a possibility, in particular, has been demonstrated in [91, 92]. Figure 22a [90] demonstrates how the angle of rotation of the skyrmion lattice changes under the action of static electric and magnetic fields of different polarities. We note that each skyrmion has an electric dipole moment [89].

In recent years, the dynamic properties of Cu_2OSeO_3 crystals have also been studied both theoretically [93–95] and experimentally [95, 96]. The magnetoelectric resonance in the multiferroic Cu_2OSeO_3 includes oscillations of not only the magnetic field vector but also the electric moment vector, which should interact with corresponding fields. To trace the effect of variable fields on the response of skyrmions in Cu_2OSeO_3, the problem was solved, first, based on the Heisenberg Hamiltonian analogous to (16) [93]. A lattice of skyrmions with a local distribution of spins was constructed. Then, to take the effects of dynamic variables into account, the Landau–Lifshitz–Gilbert equation [92, 93] was solved:

$$\frac{d\mathbf{m}_i}{dt} = -\mathbf{m}_i \times \mathbf{H}_i^{eff} + \frac{\alpha_G}{m}\mathbf{m}_i \times \frac{d\mathbf{m}_i}{dt},$$

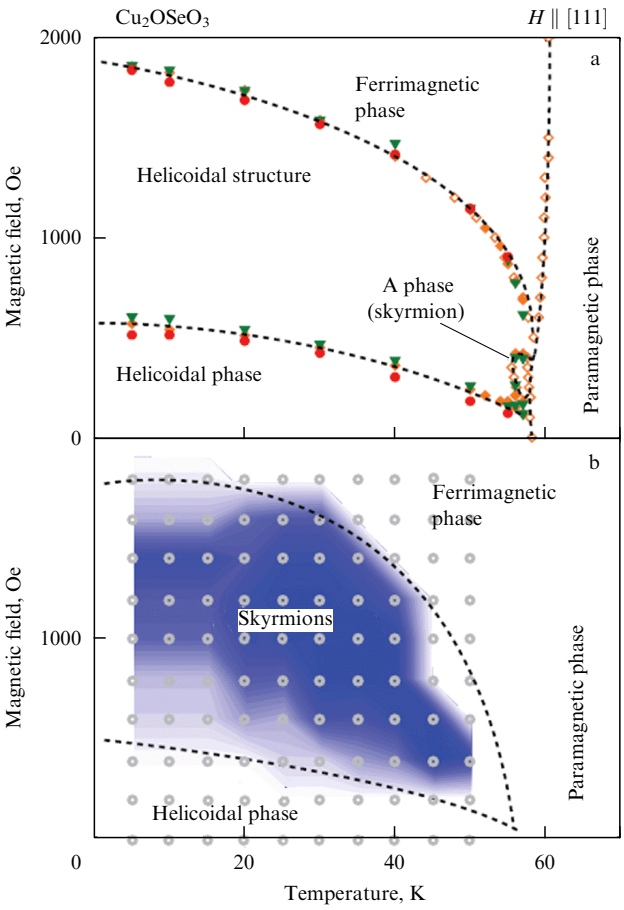

Figure 21. Phase diagram in the "applied magnetic field–temperature" coordinates for (a) a bulk sample and (b) a film of Cu_2OSeO_3 [75].

where $\mathbf{m}_i$ is the classical spin moment per the unit cell tetrahedron of the crystal, $m = |\mathbf{m}_i|$, and i runs over all tetrahedra. The effective field was calculated based on the Hamiltonian $\hat{H} = \hat{H}_0 + \hat{H}'(t)$, $\mathbf{H}_i^{eff} = -\partial\hat{H}/\partial\mathbf{m}_i$, where $\hat{H}'(t)$ is the specified disturbance; and α_G is the damping constant. The variable field $\hat{H}'(t)$ was applied and the magnetic and electric momenta were calculated for the $N \times N = 288 \times 288$ positions of Cu^{2+} ions.

The possible types of skyrmions in Cu_2OSeO_3 under the resonance microwave action are shown schematically in Figs 22 (b–d) [95]. The modes with counterclockwise (Fig. 22b) and clockwise (Fig. 22c) rotation are observed at a frequency of about 1 GHz in the fields of 250–400 Oe [95]; and the 'breathing' mode (Fig. 22d), in which the skyrmions alternately shrink and grow in size, is observed at 1.5 GHz. As can be seen from (17) (see also Section 2.6), the direction of 'twisting' in skyrmions is determined by the sign of the Dzyaloshinskii–Moriya interaction.

It has been shown in [94, 95] that the resonance interaction between the electric and magnetic systems in Cu_2OSeO_3 leads to a large 'diode' effect — different absorption of the electromagnetic wave depending on the direction of the vector $\mathbf{k}^\omega$ that characterizes the wave. This effect (≈ 20 %), which arises as a result of the excitation of the 'motion' of skyrmions, can be used in applications as a rectifier of microwave radiation. The conditions under which such a resonance phenomenon can be observed in Cu_2OSeO_3 are given in [95]: $\mathbf{k}^\omega || \mathbf{P} \times \mathbf{M}$, in particular, $\mathbf{P}||[001]$, $\mathbf{H}||[110]||\mathbf{M}$, and $\mathbf{k}^\omega||[1\bar{1}0]$. Here, $\mathbf{P}$ and

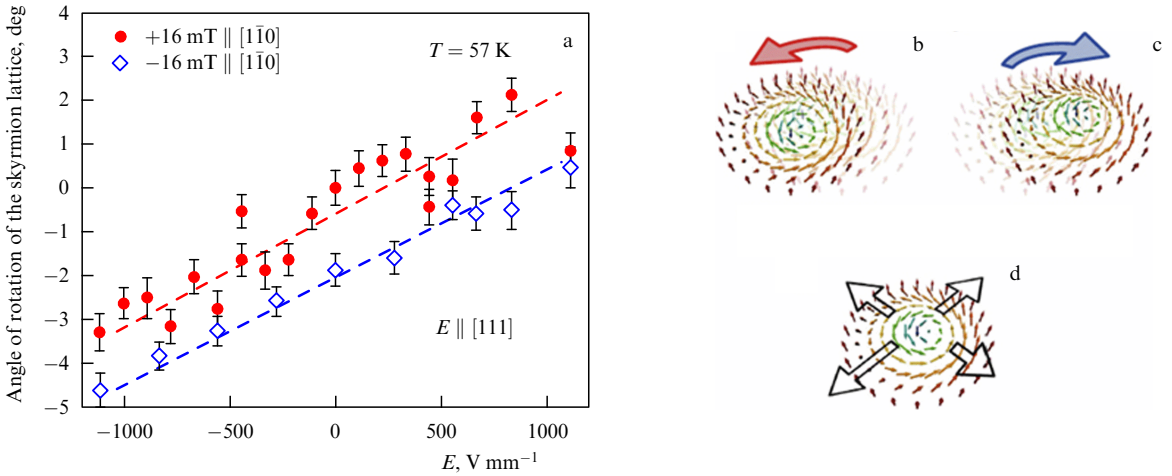

Figure 22. (a) Rotation of a skyrmion lattice ($T = 57$ K) by a static electric field ($\mathbf{E} \,||\, [111]$) in Cu_2OSeO_3 crystals [91] for two values of the constant magnetic field directed along [110]. (b–d) Arrangement of skyrmions (schematic) in the resonance state under the action of a variable magnetic field [94]: (b) counterclockwise rotation, (c) clockwise rotation, and (d) 'breathing' mode.

M are the constant parts of the respective electric and magnetic vectors.

As can be seen from the survey of phase diagrams (see, e.g., [75, 81]) and of the results of calculations (in particular, [87, 93, 94]), the condition for the appearance of skyrmions in magnetic crystalline structures such as MnSi and Cu_2OSeO_3 is the existence of a helicoidal structure at certain magnetic fields and temperatures. The source of the helicoidal structure is the competition between the Dzyaloshinskii–Moriya interaction and isotropic exchange. The presence of easy-plane uniaxial anisotropy in thin films substantially extends the region of existence of skyrmions [75, 88].

5. Conclusions

In the case of 'conventional' objects, the results presented in this review indicate the possibility of solving the problem of an independent quantitative description and prediction of the magnetic anisotropy of magnetically concentrated crystals with ions in the S state. The solution of this problem opens new possibilities for designing promising materials based on known materials in the case of the existence of isostructural crystals with lattice parameters close to those of the initial magnetically concentrated substances. The investigation methods involving diamagnetic analogs were chosen so as to avoid using extremely high (150–250 kOe) external magnetic fields in experiments on magnetically concentrated crystals (such fields are by no means always available [8, 57]).

Measurements of magnetic anisotropy in the region of the existence of a spin cycloid (in small and medium fields [8]) in $BiFeO_3$ prove to be impossible. But the anisotropy can be estimated using compositions such as $BiAl_{1-x}Fe_xO_3$ with a small content of iron (sufficient to ensure the observation of EPR spectra of single ions and pairs of ions).

It is obvious that skyrmions have been studied much less than 'conventional' structures. Nevertheless, there are quite numerous data suggesting the fundamental importance of anisotropic interactions, which in the case under consideration determine the magnetic nanostructures and the structures of 'traditional' compounds.

Certain hopes are pinned on the application of skyrmions in practice. Notably, the potential of the application of skyrmions as carriers of information and tools for its processing in magnetic memory devices has been considered in [97]. However, wide applications of skyrmions require additional theoretical and experimental investigations, including the development of means to efficiently control their behavior and the search for new materials with high Curie temperatures.

Acknowledgments

We are grateful to L M Rudenko, T V Spirina, and N V Veretennikova for the assistance in the preparation of this review. This study was supported in part by the Program of Federal Support for Leading Scientific Schools of the Russian Federation (project No. NSh 1044.2012.2); by the President's Program of Support for Leading Scientific Schools (project No. NSh-2886.2014.2); and by the Russian Foundation for Basic Research (project No. 13-02-00358).

References

1. Wolf W P *Phys. Rev.* **108** 1152 (1957)
2. Nikiforov A E, Mitrofanov V Ya, Men A N *Phys. Status Solidi B* **45** 65 (1971)
3. Kuz'menko A M et al. *JETP* **113** 113 (2011); *Zh. Eksp. Teor. Fiz.* **140** 131 (2011)
4. Pankrats A I et al. *Phys. Solid State* **50** 79 (2008); *Fiz. Tverd. Tela* **50** 77 (2008)
5. Zvezdin A K, Pyatakov A P *Phys. Usp.* **52** 845 (2009); *Usp. Fiz. Nauk* **179** 897 (2009)
6. Zvezdin A K, Pyatakov A P *Phys. Usp.* **47** 416 (2004); *Usp. Fiz. Nauk* **174** 465 (2004)
7. Pyatakov A P, Zvezdin A K *Phys. Usp.* **55** 557 (2012); *Usp. Fiz. Nauk* **182** 593 (2012)
8. Pyatakov A P, Doctoral (Phys.–Math.) Dissertation (Moscow: Moscow State Univ., 2013)
9. Dzialoshinskii I E *Sov. Phys. JETP* **5** 1259 (1957); *Zh. Eksp. Teor. Fiz.* **32** 1547 (1957)
10. Turov E A *Physical Properties of Magnetically Ordered Crystals* (New York: Academic Press, 1965); Translated from Russian: *Fizicheskie Svoistva Magnitouporyadochennykh Kristallov* (Moscow: Izd. AN SSSR, 1963)
11. Kanamori J, in *Magnetism* Vol. 1 (Eds G T Rado, H Suhl) (New York: Academic Press, 1963) p. 127
12. Rimai L, Kushida T *Phys. Rev.* **143** 160 (1966)
13. Miyata N, Argyle B E *Phys. Rev.* **157** 448 (1967)

14. Rudenko V V, Ph.D. Thesis (Phys.–Math.) (Krasnoyarsk: Physical Institute, Siberian Branch, Academy of Sciences of the USSR, 1983)
15. Bayukov O A, Rudenko V V *Sov. Phys. Solid State* **34** 1428 (1992); *Fiz. Tverd. Tela* **34** 2665 (1992)
16. Rudenko V V *Russ. Phys. J.* **52** 990 (2009); *Izv. Vyssh. Uchebn. Zaved. Fiz.* **52** (9) 92 (2009)
17. Krupička S *Physik der Ferrite und der verwandten magnetischen Oxide* (Braunschweig: Vieweg + Sohn, 1973); Translated into Russian: *Fizika Ferritov i Rodstvennykh im Magnitnykh Okislov* (Moscow: Mir, 1976)
18. Callen H B, Shtrikman S *Solid State Commun.* **3** 5 (1965)
19. Rubinshtein B E *Sov. Phys. Solid State* **11** 1592 (1970); *Fiz. Tverd. Tela* **11** 1980 (1969)
20. Al'tshuler S A, Kozyrev B M *Electron Paramagnetic Resonance in Compounds of Transition Elements* (New York: Wiley, 1974); Translated from Russian: *Elektronnyi Paramagnitnyi Rezonans Soedinenii Elementov Promezhutochnykh Grupp* (Moscow: Nauka, 1972)
21. Biedenharn L C, Louck J D *Angular Momentum in Quantum Physics: Theory and Application* (Reading, Mass.: Addison-Wesley Publ.Co., 1981); Translated into Russian: *Uglovoi Moment v Kvantovoi Fizike* (Moscow: Mir, 1984)
22. Harris E A *J. Phys C Solid State Phys.* **5** 338 (1972)
23. Heming M et al. *Solid State Comm.* **44** 543 (1982)
24. Petrakovskaya E A et al., in *Rezonansnye i Magnitnye Svoistva Magnitodielektrikov* (Resonance and Magnetic Properties of Magnetodielektrics) (Ed. G A Petrakovskii) (Krasnoyarsk: Inst. Fiziki SO AN SSSR, 1978) p. 155
25. Martynov S N, Petrov S B *Physica Status Solidi B* **149** K41 (1988)
26. Wette F W, Schacher G E *Phys. Rev.* **137** A78 (1965)
27. Rudenko V V, Khlystov A S *Russ. Phys. J.* **42** 508 (1999); *Izv. Vyssh. Uchebn. Zaved. Fiz.* **42** (5) 82 (1999)
28. Artman J O, Murphy, J C Foner S *Phys. Rev.* **138** A912 (1965)
29. Rodrigue G P, Meyer H, Jones R V *J. Appl. Phys.* **31** 376S (1960)
30. Barberis G E et al. *Phys. Rev. B* **12** 853 (1975)
31. Lukin S N et al. *Sov. Phys. Solid State* **22** 29 (1980); *Fiz. Tverd. Tela* **22** 51 (1980)
32. Rudenko V V *Sov. Phys. Solid State* **22** 453 (1980); *Fiz. Tverd. Tela* **22** 775 (1980)
33. Bondarenko G V et al. *J. Magn. Magn. Mater.* **335** 90 (2013)
34. Rudenko V V *Phys. Solid State* **36** 1377 (1994); *Fiz. Tverd. Tela* **36** 2531 (1994)
35. Morosin B *Acta Cryst. B* **28** 230 (1972)
36. Borovik-Romanov A S "Antiferromagnetizm" ("Antiferromagnetism"), in *Itogi Nauki. Fiziko-Matematicheskie Nauki* (Progress in Science. Physical and Mathematical Sciences) Vol. 4 (Ed. Ya G Dorfman) (Moscow: Izd. AN SSSR, 1962) p. 7
37. Penkala E *Zarys Krystalochemii* (Warszawa: Państwowe Wydawn. Naukowe, 1972); Translated into Russian: *Ocherki Kristallokhimii* (Leningrad: Khimiya, 1974)
38. Wanklyn B M *J. Cryst. Growth* **65** 533 (1983)
39. Sharma R R, Das T P, Orbach R *Phys. Rev.* **149** 257 (1966)
40. Chlystov A et al., in *Magnetic Resonance and Related Phenomena. Proc. of the XX Congress AMPERE, Tallinn, August 21–26, 1978* (Eds E Kundla, E Lippmaa, T Saluvere) (Berlin: Springer, 1979) p. 295
41. Abragam A, Pryce M H L *Proc. R. Soc. Lond. A* **205** 135 (1951)
42. Garifullina R L, Zaripov M M, Stepanov V G *Sov. Phys. Solid State* **12** 43 (1970); *Fiz. Tverd. Tela* **12** 55 (1970)
43. Statz H et al *J. Appl. Phys. Suppl.* **32** 218S (1961)
44. Moskvin A S, Bostrem I G, Sidorov M A *JETP* **77** 127 (1993); *Zh. Eksp. Teor. Fiz.* **103** 2499 (1993)
45. Ovchinnikov S G, Rudenko V V, Tugarinov V I *Phys. Solid State* **52** 112 (2010); *Fiz. Tverd. Tela* **52** 106 (2010)
46. Geschwind S *Phys. Rev.* **121** 363 (1961)
47. Vorotynov A, Petrakovskii G, Rudenko V *Phys. Solid State* **52** 1424 (2010); *Fiz. Tverd. Tela* **52** 1330 (2010)
48. Men'shikov V V et al. *J. Magn. Magn. Mater.* **267** 289 (2003)
49. Owen J *J. Appl. Phys.* **32** 213S (1961)
50. Garifullina R L, Zaripov M M *Sov. Phys. Solid State* **15** 1275 (1973); *Fiz. Tverd. Tela* **15** 1909 (1973)
51. Doroshev V D et al. *JETP Lett.* **29** 257 (1979); *Pis'ma Zh. Eksp. Teor. Fiz.* **29** 286 (1079)
52. Pakhomov A S, Smol'kov N A, in *Itogi Nauki. Fiziko-Matematicheskie Nauki* (Progress in Science. Physical and Mathematical Sciences) Vol. 4 (Ed. Ya G Dorfman) (Moscow: Izd. AN SSSR, 1962) p. 119
53. Vorotynov A M et al. *Phys. Solid State* **42** 1313 (2000); *Fiz. Tverd. Tela* **42** 1275 (2000)
54. Prozorova L A, Borovik-Romanov A S *Sov. Phys. JETP* **28** 910 (1969); *Zh. Eksp. Teor. Fiz.* **55** 1727 (1968)
55. Borovik-Romanov A S *Sov. Phys. JETP* **9** 539 (1959); *Zh. Eksp. Teor. Fiz.* **36** 766 (1959)
56. Borovik-Romanov A S, in *Problemy Magnetizma* (Problems of Magnetism) (Exec. Eds V A Ignatchenko, Yu V Zakharov) (Moscow: Nauka, 1972) p. 47
57. Velikov L V et al. *Sov. Phys. JETP* **39** 909 (1974); *Zh. Eksp. Teor. Fiz.* **66** 1847 (1974)
58. Bar'yakhtar V G et al., in *Tezisy 19 Vsesoyuz. Soveshchaniya po Fizike Nizkikh Temperatur* (Abstracts of the 19th All-Union Symp. on the Low-Temperature Physics) (Minsk, 1976) p. 561
59. Rudenko V V, Seleznev V N, Khlystov A S, in *Tezisy Vsesoyuz. Konf. po Fizike Magnitnykh Yavlenii* (Abstracts of the Al-Union Conf. on the Physics of Magnetic Phenomena) (Donetsk, 1981) p. 80
60. Aleksandrov K S et al. *Sov. Phys. JETP* **65** 591 (1987); *Zh. Eksp. Teor. Fiz.* **92** 1042 (1987)
61. Morrison B R, Morrish A H, Troup G J *Phys. Stus Solidi B* **56** 183 (1973)
62. Barak J, Jaccarino V, Rezende S M *J. Magn. Magn. Mater.* **9** 323 (1978)
63. Gouvea M E, Pires A S T *Phys. Rev. B* **34** 306 (1986)
64. Moriya T *Phys. Rev.* **120** 191 (1960)
65. Dmitrienko V E et al. *Nature Phys.* **10** 202 (2014)
66. Sosnowska I, Neumaier T P, Ehele S *J. Phys. C Solid State Phys.* **15** 4835 (1982)
67. Smolenskii G A, Chupis I E *Sov. Phys. Usp.* **25** 475 (1982); *Usp. Fiz. Nauk* **137** 415 (1982)
68. Mitsek A I, Smolenskii G A *Sov. Phys. Solid State* **4** 2620 (1963); *Fiz. Tverd. Tela* **4** 3581 (1962)
69. Belik A A et al. *Chem. Mater.* **18** 133 (2006)
70. Zylberberg J et al. *Chem. Mater.* **19** 6385 (2007)
71. Palewicz A et al. *Acta Phys. Polon. A* **117** 296 (2010)
72. Maruyama T et al. *Nature Nanotechnol.* **4** 158 (2009)
73. Muhlbauer S et al. *Science* **323** 915 (2009)
74. Yu X et al. *Nature Lett.* **465** 901 (2010)
75. Seki S Y et al. *Science* **336** 198 (2012)
76. Bogdanov A N, Yablonskii D *Sov. Phys. JETP* **68** 101 (1989); *Zh. Eksp. Teor. Fiz.* **95** 178 (1989)
77. Heinze S et al. *Nature Phys.* **7** 713 (2011)
78. Stishov S M, Petrova A E *Phys. Usp.* **54** 1117 (2011); *Usp. Fiz. Nauk* **181** 1157 (2011)
79. Neubauer A et al. *Phys. Rev. Lett.* **102** 186602 (2009)
80. Harada K et al. *Nature* **360** 51 (1992)
81. Demishev S V et al. *JETP Lett.* **93** 213 (2011); *Pis'ma Zh. Eksp. Teor. Fiz.* **93** 231 (2011)
82. Corti M et al. *Phys. Rev. B* **75** 115111 (2007)
83. Demishev et al. *Phys. Rev. B* **85** 045131 (2012)
84. Moriya T *Spin Fluctuations in Itinerant Electron Magnetism* (Berlin: Springer-Verlag, 1985)
85. Jeong T, Pickett W *Phys. Rev. B* **70** 075114 (2004)
86. Glushkov V V et al. *JETP* **99** 394 (2004); *Zh. Eksp. Teor. Fiz.* **126** 444 (2004)
87. Chizhikov V, Dmitrienko V *Phys. Rev. B* **85** 014427 (2012)
88. Karhu E et al. *Phys. Rev. B* **85** 094429 (2012)
89. Seki S, Ishiwata S, Tokura Y *Phys. Rev. B* **86** 060403 (2012)
90. Adams T et al. *Phys. Rev. Lett.* **108** 237204 (2012)
91. Seki S et al. *Phys. Rev. B* **85** 220406(R) (2012)
92. White J S et al. *J. Phys. Condens. Matter* **24** 432201 (2012)
93. Mochizuki M *Phys. Rev. Lett.* **108** 017601 (2012)
94. Mochizuki M, Seki S *Phys. Rev. B* **87** 134403 (2013)
95. Okamura Y et al. *Nature Commun.* **4** 2391 (2013)
96. Onose Y et al. *Phys. Rev. Lett.* **109** 037603 (2012)
97. Nagaosa N, Tokura Y *Nature Nanotechnol.* **8** 899 (2013)